ENERGY MODELING OF WEARABLE INTELLIGENT BATTERYLESS HEALTH MONITORING SYSTEM WITH THERMAL-VIBRATIONAL HYBRID HARVESTER

A THESIS SUBMITTED TO
THE BOARD OF GRADUATE PROGRAMS
OF
MIDDLE EAST TECHNICAL UNIVERSITY, NORTHERN CYPRUS CAMPUS

BY

MOLLY SHARONE

IN PARTIAL FULFILLMENT OF THE REQUIREMENTS
FOR
THE DEGREE OF MASTER OF SCIENCE

IN SUSTAINABLE ENVIRONMENT AND ENERGY SYSTEMS PROGRAM

SEPTEMBER 2021

Approval of the Board of Graduate Programs

Prof. Dr. Cumali Sabah
Chairperson

I certify that this thesis satisfies all the requirements as a thesis for the degree of Master of Science

Asst. Prof. Dr. Ceren İnce Derogar
Program Coordinator

This is to certify that we have read this thesis and that in our opinion it is fully adequate, in scope and quality, as a thesis for the degree of Master of Science.

Prof. Dr. Ali Muhtaroğlu
Supervisor

Examining Committee Members:

Prof. Dr. Elif Uysal
Electrical and Electronics Eng., METU

Prof. Dr. Ali Muhtaroğlu
Electrical and Electronics Eng., METU NCC

Assoc. Prof. Dr. Enver Ever
Computer Eng., METU NCC

Asst. Prof. Dr. Meryem Erbilek
Computer Eng., METU NCC

Asst. Prof. Dr. Neyre Tekbıyık Ersoy
Energy Systems Eng., CIU

I hereby declare that all information in this document has been obtained and presented in accordance with academic rules and ethical conduct. I also declare that, as required by these rules and conduct, I have fully cited and referenced all material and results that are not original to this work.

Name, Last name : Molly Sharone

Signature:

ABSTRACT

ENERGY MODELING OF WEARABLE INTELLIGENT BATTERYLESS HEALTH MONITORING SYSTEM WITH THERMAL-VIBRATIONAL HYBRID HARVESTER

Sharone, Molly
Master of Science, Sustainable Environment and Energy Systems Program
Supervisor: Prof. Dr. Ali Muhtaroğlu

September 2021, 102 pages

A unified model is developed in this thesis with a thermal-vibrational hybrid energy harvester and a wearable intelligent batteryless health monitoring system for accurate prediction of energy flow from generation to consumption. Analytical models are developed first based on environmental conditions, energy conversion parameters, geometry, and datasheet specifications. Data from literature is utilized from multiple energy harvesters, interface electronics, the intelligent sensor nodes and monitored patients to tune correlation factors for model accuracy. The resulting system level framework, named HeMeS, effectively enables the development of wearable batteryless sensor systems across a large design space by investigating tradeoffs among operation conditions, processing and transmission performance, size, and cost. Multiple threads of analysis have been successfully showcased using HeMeS to demonstrate convergence to an optimized autonomous (batteryless) system design with hybrid thermal and vibrational energy harvesting under a variety of environment, cost, size and patient constraints applicable to different health monitoring WBAN nodes.

Keywords: Energy harvesting; Piezoelectric harvesting; thermoelectric generation; energy harvesting system models, WBAN power system modeling.

ÖZ

TERMAL-TİTREŞIMLİ HİBRİT HARVESTER İLE GİYİLEBİLİR AKILLI PİLSİZ SAĞLIK İZLEME SİSTEMİNİN ENERJİ MODELLEMESİ

Sharone, Molly
Yüksek Lisans, Sürdürülebilir Çevre ve Enerji Sistemleri
Tez Yöneticisi: Prof. Dr. Ali Muhtaroğlu

Eylül 2021, 102 safya

Bu tezde, üretimden tüketime enerji akışının doğru tahmini için termal-titreşimli hibrit enerji toplayıcı ile giyilebilir akıllı pilsiz sağlık izleme sisteminden oluşan birleşik bir model geliştirilmiştir. Analitik modeller önce çevresel koşullara, enerji dönüşüm parametrelerine, geometriye ve veri sayfası özelliklerine dayalı olarak geliştirilmiştir. Model doğruluğunu ve korelasyon faktörlerini ayarlamak için literatürden elde edilen veriler, çoklu enerji toplayıcılarından, arayüz elektroniklerinden, akıllı sensör düğümlerinden ve izlenen hastalardan elde edilmiştir. HeMeS olarak adlandırılan bu sistem, giyilebilir pilsiz sensör sistemlerinin geliştirilmesine olanak sağlarken aynı zamanda çalışma koşulları, işleme ve iletim performansı, boyut ve maliyet arasındaki farkları da araştırarak geniş bir tasarım alanında faaliyet gösterebilir. Farklı WBAN sağlık izleme düğümlerine uygulanabilir çeşitli ortam, maliyet, boyut ve hasta kısıtlamaları altında hibrit termal ve titreşimsel enerji toplama ile optimize edilmiş otonom (pilsiz) bir sistem tasarımına yakınsamayı göstermek için HeMeS kullanılarak birden fazla analiz dizisi başarıyla sergilendi.

Anahtar Kelimeler: Enerji hasatlaması, Piezoelektrik hasatlamasi, Termoelektrik üretimi, Enerji hasat sistemi modeleri, WBANgüç systemin modellemesi

This thesis is dedicated to my grandmother Agnes Adhiambo and my parents, whose hard work gave me a decent education.

ACKNOWLEDGMENTS

Conducting an impactful and significant thesis is hard work that would have been impossible without continued guidance, and support from my supervisor, Professor Dr. Ali Muhtaroğlu. His passion for innovative and sustainable health monitoring provided a common ground to work together and taught me a great deal in the process. I also thank him for being so patient with me when I struggled with deadlines. His consistency was truly admirable. Working with him was a huge privilege and I am forever indebted to him.

I would like to thank Prof. Dr. Elif Uysal, Asst. Prof. Dr. Neyre Ersoy, Assoc. Prof. Dr. Enver Ever, Asst. Prof. Dr. Meryem Erbilek for being part of my thesis defense committee and for giving suggestions for improvement areas in this work.

I would also like to thank the entire SEES department for teaching me about energy harvesting and the urgency of implementing sustainable practices for a greener world.

My deep gratitude goes to Middle East Technical University Northern Cyprus Campus' (METU NCC) administration, for the graduate teaching and research scholarship, which funded my graduate studies.

I also thank Hon. Engineer Philip Okundi and Ian Okundi for their financial support during my entire stay abroad. In addition, I thank them for the educational mentorship and for directing my steps to METU. I also thank My parents Maurice Orinda and Judith Orinda, for their efforts that brought me this far.

I have been blessed with a strong support system through my friends, Esther, Hope, Yewande, Shima, Millicent, Zehra, Sena, Johnstone, and siblings Edwina, Reagan and, Naomi. Their emotional support was paramount and kept me motivated.

Lastly, I would like to thank *mudiwa* Honest Jimu for the love and friendship and Mike Arasa for always challenging me to work harder.

TABLE OF CONTENTS

LIST OF TABLES

TABLES

LIST OF FIGURES

FIGURES

LIST OF ABBREVIATIONS

ABBREVIATIONS

BP- Blood pressure

CPU- Central Processing Unit

CSS- Cascading Style Sheets

ECG-Electrocardiograph

EEG- Electroencephalogram

EH- Energy Harvesting

EMG- Electromyograph

FUC- Frequency Up Conversion

HeMeS- Health monitoring energy system tool

HMS -Health monitoring system

PPG - Photoplethysmography

PVDF- Polyvinylidene fluoride

PDA- Personal Digital Assistant

PIC- Programmable Intelligent Computer

TEG- Thermoelectric generator

WBAN-Wireless body area networks

CHAPTER 1

INTRODUCTION

1.1 Wireless Body Area Network (WBAN)

Technological advancements in microelectronics, integrated circuits, wireless communication, internet of things and intelligent low power sensors have opened a gateway for the development of Wireless Body Area Networks (WBANs) [1],[2]. A wireless body area network comprises of miniaturized, wearable or implantable, low power, lightweight sensor nodes that are strategically placed at various points in/on the human body [3]. These WBANs have found applications in various fields such as entertainment, fitness tracking and telemedicine/health monitoring, among others [4].

Health monitoring WBANs have experienced a rapid development in the recent years which has in turn revolutionized how health professionals practice medicine [5],[6]. Patients can be monitored for chronic diseases continuously and unobtrusively in their normal day to day environment, providing instant or early communication with the doctors and healthcare facilities as frequently as necessary [7]. This results in the development of unobtrusive health monitoring solutions as outlined in [8]. WBANs can be used to develop intelligent and affordable smart healthcare systems including diagnostics and treatment of chronic conditions in various individuals. Figure 1.1 presents a conceptual diagram of a WBAN-based health-care system. The figure shows various sensor nodes spread all over the body of a human being to measure specific bio signals. After the health data has been collected at a gateway node such as a mobile device, it is transmitted to a database where it can be accessed by care givers or doctors.

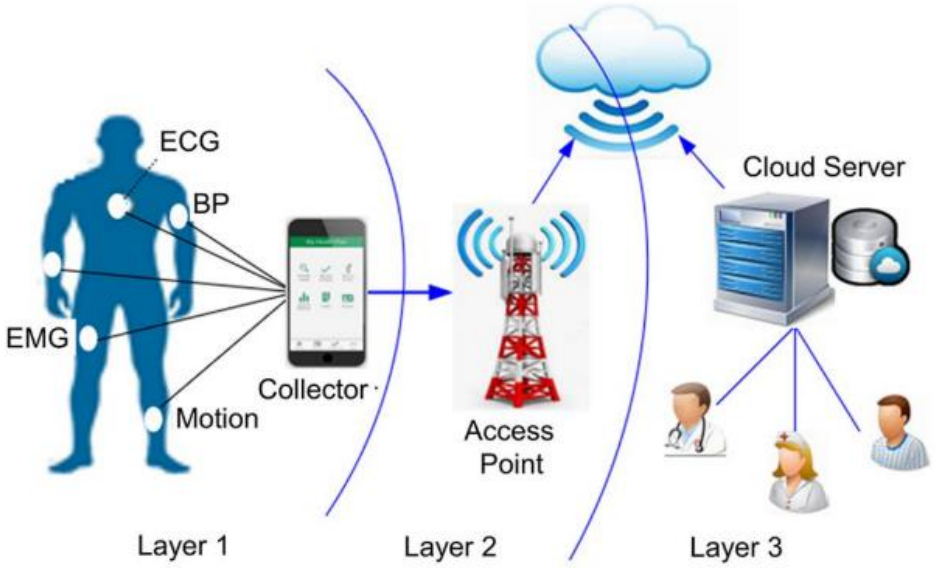

Figure 1.1. Conceptual diagram of a WBAN-based health care system [9].

Healthcare integration is a prominent aspect of future sustainable smart cities [10]. Each node in a health monitoring WBAN typically sense one or more physiological parameters such as electrocardiogram, blood sugar/glucose concentration, heart rate, temperature and pressure through sensors, use a microcontroller for signal processing and conditioning, and include a communication device such as a transceiver and a power management unit [11] for effective delivery of power to various components. Figure 1.2 shows a diagram of a typical sensor node. The overall system can be integrated into day-to-day wearable structures such as clothes, shoes, badges, belts or bracelets [12].

1.2 Communication standards for health monitoring systems

After biological signals are measured and processed, associated data is transmitted to a central location, for example, the physicians computer or the database of a medical station [13]. With the development of faster communication infrastructure such as 5G, health monitoring systems will be able to communicate at higher data rates. However, there is a direct relationship between communication bandwidth and

power dissipation, as will be discussed in the next section. The most common communication standards in WBANs so far are Bluetooth (IEEE 802.15.1) and Zigbee (802.15.4), which will be briefly described next.

i) Bluetooth

Bluetooth is used for short-range RF-based connectivity between portable and non-portable devices. It is a low-power and cost-effective RF standard with an operating frequency of 2.4 GHz with about 10 m transmission distance typically. Bluetooth systems can be categorized into two broad classes, namely:

- Classic Bluetooth system which conforms to the versions before the 4.0 Bluetooth specification. It can also be referred to as Basic Rate (BR) when the device supports up to a maximum of 721 kbps or Enhanced Data Rate (EDR) if the device can support up to 2.1 Mbps.
- Low Energy system that is based on the 4.0 or higher version of Bluetooth specification and is compatible with ultra-low power applications. Bluetooth Low Energy (BLE) has lower structural complexity and cost in comparison to the classic BR/EDR versions of Bluetooth. BLE's maximum data rate is 305 kbps for 4.0 versions and up to 800 kbps for 4.2 compliant devices. Application areas for BLE are quite vast because it conforms to the already existing Bluetooth ecosystem and addresses the needs in low consumption devices. This version is therefore better suited for data transmission in autonomous wearable health monitoring systems [14].

ii) Zigbee

The Zigbee aims at low-cost, low data-rate systems with long lasting battery life, and simple structures. It also has a transmission range of approximately 75 m at a frequency of 2.4 GHz. Zigbee has lower data rates compared to Bluetooth [15].

Some other short range communication modules include infrared (IrDA) [16], and Medical Implant Communication Service (MICS) [17]. Table 2.2 summarizes

various features of the above-described communication standards. Presented power consumption denotes the amount of power consumed when the module is active.

Table 1.1. Communication standards for WBANs [13]–[15]

Module	Typical range	Data rate	Typical power consumption	Frequency
Zigbee	10 - 75 m	20 kbps / 40 kbps / 250 kbps	30 mW	868 MHz / 915 MHz / 2.4 GHz
Bluetooth (Classic)	10 - 100 m	1 - 3 Mbps	1 W (max)	2.4 GHz
BLE	30 - 100 m	305 - 805 kbps	10 - 500 mW	2.4 GHz
MICS	2 m	500 Kbps	25 µw	402 - 405 MHz
802.11g	200 m	54 Mbps	1 W	2.4 GHz

1.3 Energy Issues in WBANs

Powering health monitoring WBANs require a reliable energy source to ensure efficient performance of the sensor nodes. Traditionally, these devices have been powered using batteries and for consumers the longevity of the battery life is one of the key factors to consider before making a purchase [18].

Some of the batteries used to power health monitoring systems include the non-rechargeable CR2032 and CR3032, or rechargeable lithium-ion, lithium-polymer, nickel-metal-hydride, lithium-manganese, or lithium-ion-phosphate. A rechargeable battery needs a charger circuit, which further contributes to size and cost. The depletable nature of batteries has proven to be problematic in biomedical applications [19], [20].

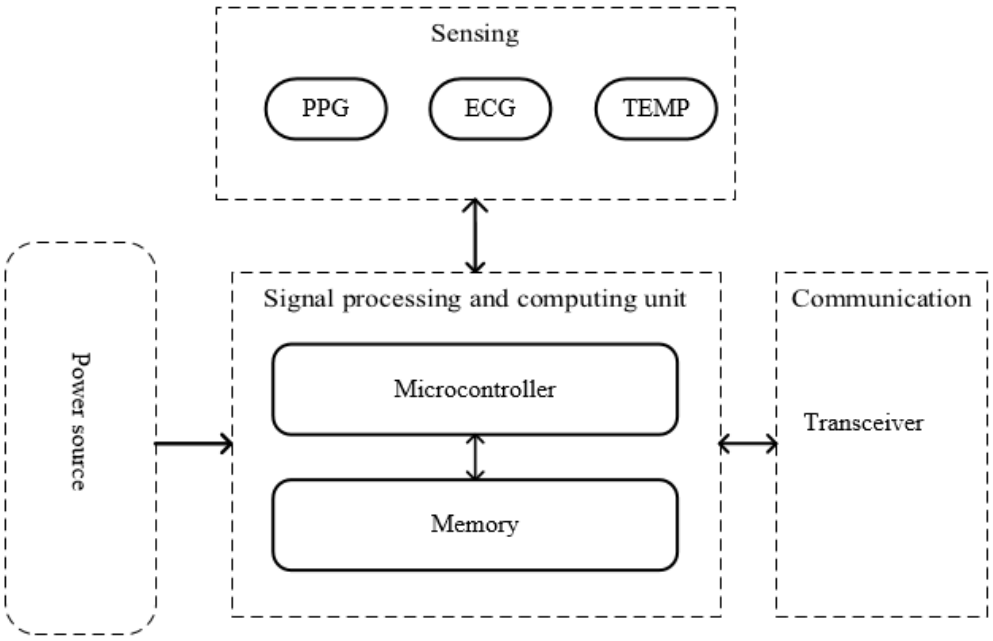

Figure 1.2. A typical WBAN health monitoring sensor node

When the batteries are depleted due to limited lifetime, the health monitoring devices become useless until the batteries have been replaced or recharged [20]. Additionally, the location of the sensor nodes may not allow for the possibility of battery replacement [21]. Such limitations can pose dangerous risks on the monitored patients or lead to inconsistent data. One popular method used to increase the battery lifetime through duty-cycling in the system components i.e., example, when in duty cycling mode, the communication system and the biosensors operate in the following manner: Once the control information is received from the central processing unit, the biosensor is switched from standby (sleep) mode to active mode before the transmission period. During the active mode, the signal sensed by the wearable biosensor is transmitted to the CPU across the communication link around the human body. After transmission of the sensed data, the biosensor would switch to standby for energy saving, and at this time, most of the transceiver circuits are powered off [22], [23]. This technique can only lengthen the lifetime of the electrochemical power source without offering a quasi-perpetual solution. Uninterrupted sensing and

transmission of health data, however, necessitates energy autonomy in wearable systems [24].

Energy autonomy not only avoids disruptions in WBAN operations but can also eliminate the need to replace batteries frequently. Therefore, energy harvesting is a promising area for fully autonomous WBANs [25].

1.4 Energy harvesting for health monitoring WBANs

Energy harvesting (EH) is the process of transducing ambient energy, which would otherwise be wasted, into usable electrical power [19]. Some typical sources of harvestable energy include wind, solar, vibrations, thermal, radio frequency (RF) waves [5],[26],[27]. Unlike harvesting energy from machines, EH from the human body is more complicated because of the limited size of the harvester and the low frequency of human body motion [25]. Consequently, only a low amount of power can be harvested from body-based transducers. Luckily, while Moore scaling has enabled small-sized ultra-low-power WBANs, system design techniques such as transmission schedules have reduced energy requirements. These developments allow for the feasibility of EH for complete autonomy in at least a subset of WBANs [28].

1.4.1 Hybrid energy harvesting

To power WBANs, the total energy requirement of the WBAN must be met by the power source. When one harvester is insufficient, a hybrid configuration can be incorporated. Hybrid systems combine the advantages of multiple harvesters and address the intermittency of power generation from individual EH sources by summing their output for a higher total output average power [29].

1.4.2 Designing fully autonomous health monitoring WBANs

A self-powered health monitoring system can be designed by modeling a harvester system whose average output power is equal to the average power dissipation requirements of the sensor nodes and all the average loses. Autonomous operation

can be targeted along with optimization of size and cost by understanding system usage model, building proper models, and analyzing design trade-offs before final implementation.

1.5 Research Objectives

No comprehensive system model and tool is available in the literature so far that can investigate the generation-to-consumption energy flow within a self-powered, wearable health monitoring system that may be powered by one energy harvester or multiple (hybrid) energy harvesters working jointly. This thesis aims to fill this gap by first developing a Health-Monitoring Energy System (HeMeS) tool, which provides a unified electrical model to accurately analyze full energy flow in an autonomous WBAN node, using a thermal-vibrational hybrid energy harvester for initial power generation studies. Analytical power generation, conversion and delivery models, environmental conditions, geometry, and load requirements are simultaneously incorporated to explore system design space for a variety of health-monitoring WBAN applications.

1.6 Research contributions

Upon completing the development of the unified model health monitoring energy system tool which can be used to study the power flow from harvester(generation) side to the load consumption side, the developed tool will allow for:

- feasibility analysis of novel wearable applications involving energy harvesting.
- The study will allow for a better understanding of energy flow in the whole system of a WBAN network for accurate design.
- Understanding the energy flow in these self-powered autonomous WBANs allows for early detection of possible sources of energy waste in such system.

- A tool like HeMeS is a good starting point in the design process for autonomous health monitoring system.
- The demonstrated design space exploration using HeMeS will also enables a multidisciplinary understanding of the trade-off between environmental requirements for autonomous operation in self-powered systems verses the system capacity under certain environmental conditions.

This chapter introduced health monitoring WBANs and their importance in sustainable development in health care. It also provided an overview of the energy issues in health monitoring WBANs and how the issues can be solved through energy harvesting and system optimization. The objective of this thesis work and the thesis contribution concluded this chapter.

Chapter 2 reviews background literature on health monitoring systems in detail, their communication standards, energy harvesters as power supplies, and problems associated with existing prediction models and design tools for full-system behavior of autonomous WBAN systems. The chapter finally discusses existing system research in autonomous health monitoring including scope of application.

Chapter 3 discusses the proposed autonomous health monitoring system tool, underlying models, system architecture and implementation. In addition, this chapter defines the methodology through which the design space exploration is done using HeMeS. Various patient profiles and environmental constraints and general constraints under which the study is done is defined.

The proposed tool is utilized in Chapter 4 to demonstrate its application to explore design space under a variety of environment, cost, size, and user constraints.

Finally, Chapter 5 concludes the thesis and discusses future work.

CHAPTER 2

BACKGROUND

2.1 Introduction

The development of health monitoring systems (HMS) have recently sparked attention to mitigate the constantly increasing health cost [30]. Fortunately, due to technological advancements, miniaturized biosensors, low power microelectronics, wireless communication and smart textile have become ubiquitous [31]. Such developments have motivated scientist to develop cost effective, intelligent health monitoring systems [13]. Typical health monitoring devices are made up of physiological health sensors for measuring the biological signals, a signal processing unit such as a microcontroller, a transmission module for sending and receiving data, and a power source for the entire system as previously described in Chapter 1 (Figure 1.2). This chapter covers background on physiological sensors, including the signals measured by these sensors, different categories of health monitoring devices, and efforts in modeling health-monitoring WBAN nodes.

2.2 Physiological sensors for health monitoring

Human body health is characterized by four main vital signs which are blood pressure, temperature, pulse rate, and rate of respiration [32]. These signals are the fundamental components around which patients, especially hospitalized ones, are monitored. Even though the signs can be used as the initial reference point when a patient is being diagnosed, some additional signals from the body such as heart rate, electrocardiogram (ECG) [33], blood oxygen saturation (SO_2) [34], electro-myogram (EMG) [35], and electroencephalogram (EEG) [36] are utilized to further monitor different types of diseases in patients. These sensors are regularly applied in patient post-surgical monitoring. Additionally, motion sensing has become

important especially in monitoring the elderly and patients undergoing physiotherapy [37]. Table 2.1 summarizes various biological signals, corresponding sensors, and data.

Table 2.1. Bio signals and the corresponding bio sensors

Biological signal	**Type of sensor**	**Measured data description**
Electrocardiogram	Chest electrodes	Electrical activity of the heart
Blood pressure (systolic and diastolic)	Arm cuff-based monitor	Force exerted by circulating blood on the walls of blood vessels
Body and skin temperature	Temperature probe/skin patch	Measure of body's ability to generate and dispense heat
Respiration rate	Piezoelectric sensor	Inspiration and expiration per unit time
Oxygen saturation	Pulse oximeter	Amount of oxygen present in a patient's blood
Heart rate	Galvanic skin response	Frequency of the cardiac cycle
Blood glucose	Phonocardiograph	Measurement of amount of glucose in blood
Electromyogram (EMG)	Strip-base glucose meters	Electrical activity of the skeletal muscles
Electroencephalogram (EEG)	Skin electrodes	Measurement of electrical spontaneous brain activity
Body motion	Accelerometer	Measurement of acceleration forces in 3D

2.3 Categories of health monitoring systems

Health monitoring systems can be categorized into four different groups, including those that are microcontroller based, smart textile based, body area network (BAN) based, or custom hardware based [13].

2.3.1 Microcontroller based health monitoring systems

This category includes wearable systems that are based on a microcontroller board. All the physiological data is collected by sensors and then transmitted through wires for processing on the microcontroller board [13]. Examples of these systems in literature are as discussed below.

i) LiveNet

The Media Laboratory of MIT, Cambridge, developed a flexible distributed mobile platform aimed for long-term health monitoring with real-time data processing and streaming [38]. The components of LiveNet include Linux-based PDA mobile device, a modular sensor hub for gathering, processing, and interpreting real-time contextual data and an integrated physiological board, which incorporates a 3- axis accelerometer, an electrocardiogram (ECG), an electromyogram (EMG), and skin conductance sensors, LiveNet can also be seamlessly interfaced with a range of commercially available sensors.

ii) AMON

Anilker et al. [30] developed a wrist-worn wearable multiparameter monitoring and alert system, which can measure skin temperature, blood pressure, oxygen saturation and a single lead ECG, a 2-dimension accelerometer used for comparing patient/user activity to the measured physiological data. A GSM-based cellular communication link was also developed with a software package connected to a health center to allow physician to analyze the collected data. AMON targeted patients with cardiac and respiratory problems. Data can be collected both at the comfort of the patient's home or when confined in a medical facility.

iii) RTWPMS

Lin et al. developed and implemented Real-Time Wireless Physiological Monitoring System (RTWPMS), based on a wireless low power 2G phone and a custom physiological measuring module which measures heart rate, body temperature and

blood pressure [39]. RTWPMS additionally incorporates a GPS system and serial port for sensor interfacing. A wireless base station is also included for data transmission and overall system control. RTWPMS is mainly used in nursing homes.

iv) LifeGuard

Mundt et al. designed a multiparameter wearable physiological monitoring system for terrestrial and space applications mainly for observing the crew's respiration, electrocardiogram, heart rate, oxygen saturation, body temperature and pressure, and motion of the crew otherwise known as crew physiologic observation device [40]. Lifeguard uses typical off-the shelf sensors to measure bio signal. The signals are then transmitted to a data logger through wires and can then be sent to a base station via Bluetooth or stored for up to 9 hours in a memory card. A PIC micro-controller is implanted for the Data logger. Two AAA batteries are used to power the data logger

v) MYsignals

MYsignals is a commercially available e- health development platform that connects up to 15 sensors health monitoring sensors. Health data gathered by the developer is encrypted and sent through either ethernet or Wi-fi developer's private account at the Libelium cloud which is MYsignals manufacturer or a developer's private cloud. The collected data can be visualized using a mobile phone app, my signals website or through a customized display. MYsignals has been used for remote monitoring with a diverse case study of patients from North Africa to improve medical assistance in under staffing instances, in the Dominican Republic to help reduce maternal deaths and for promoting healthy lifestyle in work environments. Saha and Biswas developed in [41]. A Mysignals-based prototype for application in health vitals to facilitate remote patient monitoring for Covid-related symptoms. Mohammad et al. also developed a an IoT connected based LoRa wireless sensor network for human body health monitoring used MYsignal's development shield in [42].

2.3.2 Smart textile-based health monitoring systems

Garments such as t-shirts or vests can be integrated with biosensors for health monitoring. Such technology-aware garments are collectively referred to as smart textile [43]. Examples of such health monitoring systems are discussed in this section.

i) MyHeart project

This project aimed fighting cardiovascular ailments through monitoring for early diagnosis. The sensing modules in MyHeart project are embedded on clothing or integrated with the garment [44]. Tiny conductive wires are knitted in form of normal yarns in clothing. Such integration reduces the overall system size and is extremely comfortable for users. Biosensors included in MyHeart project are an ECG and an accelerometer. No wireless modules are required and a single power supply on the body controls the whole system.

ii) Wearable Health Care System (WEALTHY) project

Paradiso et al. implemented a wearable garment that covers the whole upper body and is worn beneath day-to day clothing [45]. The WEALTHY garment is capable of tracking biochemical variables and some physiological signals. The system targets patients in rehabilitation and other high-risk individuals such as the elderly. Conducting piezoresistive materials are used to integrate the sensors into fabric form. Measured physiological signals include 3-lead ECG, arm-located EMG, body motion and position, skin and body temperature, blood pressure and the thoracic and respiration rate. Bluetooth and GPRS are among the communication modules included.

iii) Hexoskin

The Hexoskin Smart Garments are commercially available textile sensors which are embedded into comfortable garments for precise and continuous cardiac, respiratory,

and activity monitoring. The users of Hexoskin garments can visualize, report, and analyze their data with the leading Hexoskin Connected Health Platform. Many scientific publications have included Hexoskin smart garments including a study done by [46] to validate the wearable vest for various activities. Elliot et al. also conducted a study to demonstrate the reliability of the Hexoskin wearable vest on its maximal aerobic power testing for elite cyclists [47].

iv) MagIC system

This is a washable vest that includes textile sensors for respiration, ECG, and motion [48]. A board is included for signal processing and an additional communication channel through Bluetooth to transfer the data to a local base station for diagnosis. MagIC is mostly used for monitoring the elderly and cardiac patients.

2.3.3 Body area network (BAN)-based health monitoring systems

These are wirelessly enabled nodes that form a body area network, and every node is responsible for collecting one or more types of physiological data and transmitting them to a central node or base station. Hao and Foster present a detailed review on BAN systems in [49].

Milenkovic et al. developed a wearable wireless body area network consisting of off-the-shelf wireless sensor network platform with IEEE 802.15.4 (Zigbee) transceiver and ultra-low power micro-controller [50].

CodeBlue[51], was developed by Harvard researchers as a multi-patient medical sensor platform using communication standards such as Zigbee and MicaZ. The system had additional custom biosensor board for measuring ECG, Pulse oximetry and motion.

In [52] a wireless body sensor network was designed and implemented based on medical implant communication service band (MICS). The system consists of a temperature sensor, pulse rate sensor, a control unit and receiver medical station. The

system is implemented to achieve low power operation using heavy duty cycling with measurements taken only every 5-10 minutes.

A research project (Human++) conducted in the Netherlands developed a WBAN with three sensor nodes with each node independently powered to acquire, condition and transmit the data wirelessly in a multichannel fashion. The system can collect ECG, EEG, and EMG data autonomously for 3 months with power supplied through AA batteries [53].

With relentless growth in internet-of-things (IoT) and machine-to-machine (M2M) interfaces, it is inevitable that most smart monitoring systems will act as a node in a wireless body area network. Hence, this category will be the focus of the thesis.

2.3.4 Custom hardware-based health monitoring systems

These types combined different types of configurations into one in a unique way. Two examples from literature of custom based HMS are:

i) Health care system developed by Chung et al. in [54] which consists of 802.15.4 capable nodes interfaced with ECG and BP sensors with cell phone display. The system's novelty and custom nature is the fact that it transmits only suspicious blood pressure or ECG signals to the hospital base station.

ii) Yuce et al.'s [52] custom based health monitoring system is based on the medical implant communication service band with temperature and pulse rate sensors in the nodes. The system had a receiver at a medical center. The system also implements heavy duty cycling where the system is mostly in sleep mode to ensure low power consumption.

Most of the health monitoring systems demonstrated above are powered using batteries. With the advent of low power sensors, these health monitoring systems can be optimized for low power applications to allow for autonomous operation through human body energy harvesting.

2.4 Power supply and management

The most critical component in a health monitoring device is its power supply [31]. Until recently, most health monitoring systems have been powered using batteries. However, this trend is changing due to aggressive research in the energy harvesting field, which aims to replace the depletable unsustainable batteries with fully energy-autonomous systems [19], [29], [55]. Depending on the power source, the induced voltages from various sources may require rectification if AC type, and stepping up or down to the required level by the loads [21]. These contribute to losses in the system due to inefficiencies from various interface electronics.

Power is dissipated due to switching of intrinsic semiconductor capacitance while signals are propagated through circuits. This category of power consumption, named active power, is directly proportional to the activity factor, frequency of switching, and has quadratic relation to voltage supply, as in Equation (1)

$$P = CV^2 f \ , \tag{1}$$

Where *C* is the switching parasitic and load capacitance, *V* is the supply voltage and *f* denotes the switching frequency.

When systems do not have active switching, they still consume static power due to DC-biased circuits and semiconductor leakage currents. This category of power dissipation is typically much lower than active power.

A good power supply and management unit is designed to minimize the losses as much as possible and offer a long-lasting energy source to the loads. Therefore, design techniques will in general ensure the activity of system components are minimized as much as possible, through due diligence in studying the requirements of system usage model. In addition, energy harvesting has been proposed as an attractive power management mechanism for mobile computing systems by Muhtaroğlu et al. [56], and has been widely investigated within the last two decades

2.5 Energy Harvesting for health monitoring systems

Energy harvesting for health monitoring systems is becoming feasible due to the development of ultra-low power microelectronics which can be safely sustained using power in the ranges of microwatts to milliwatts [6], [57], [58]. Some of the most common harvesting methods for health monitoring applications include thermoelectric (TE) harvesting, piezoelectric (PZ) harvesting, electromagnetic (EM) harvesting, Radio-Frequency (RF) harvesting and Photovoltaic (PV) solar [19]. Table 2.3 summarizes the characteristics of various energy harvesting methods. Piezoelectric harvesting and thermoelectric harvesting are discussed in detail in the following discussion, since these two categories are the most relevant to the indoor WBAN applications that is the focus of this work.

Table 2.2. Energy harvesting methods and their characteristics [19]

	PZ	**TE**	**EM**	**RF**	**PV**
Power density	10 - 200 $\mu W/cm^3$	50 - 100 $\mu W/cm^2$ per ^oC	1 - 2 $\mu W/cm^3$	0.0002 - 1 $\mu W/cm^2$	Outdoor: 100 mW/cm^2 Indoor: < 100 $\mu W/cm^2$
Output voltage	10 – 20 V (Open circuit)	10 - 100 mV	Approx. 100 mV	3 - 4 V (Open circuit)	0.5 V max
Availability	Hz - kHz frequency vibrations	Availability of temperature gradient	Hz vibration	Vicinity of radiation	Lightened environment
Pros	High voltage, Well developed technology	Non-intermittent / Less intermittent	Well developed	Antenna can be integrated, Widely available	High power density, Well-developed technology
Cons	Highly variable output, large area High output impedance	Low output voltage	Bulky, low power density, Low output voltage	Sensitive to the distance of the RF source	Intermittent, highly dependent on light

2.5.1 Piezoelectric energy harvesting

Piezoelectricity is the accumulation of electric charge due to applied mechanical stress in non-centrosymmetric crystal structures [59]. Materials with such structures are collectively referred to as piezoelectric materials. Lead zirconate titanate (PZT) and polyvinylidene difluoride (PVDF) are two common functional materials for piezoelectric energy harvesters. Compared with rigid, brittle, and heavy PZT, PVDF has considerable flexibility, good stability, and easiness to handle and shape [60].

In addition to material choice, the direction of polarization is another critical factor that influences the type of harvester suitable for a particular application. Therefore, a Cartesian coordinate system is established to identify the directions within a piezoelectric unit, as outlined in Figure 2.1. 1-axis and 3-axis represent the mechanical stress direction and polarization direction in a piezoelectric harvester, respectively [61]. In 31-mode, force is applied along the 1-axis, and charges accumulate on the 3-axis. However, in 33-mode, force is applied in 3-axis, and charges are also generated in 3-axis parallel to the force.

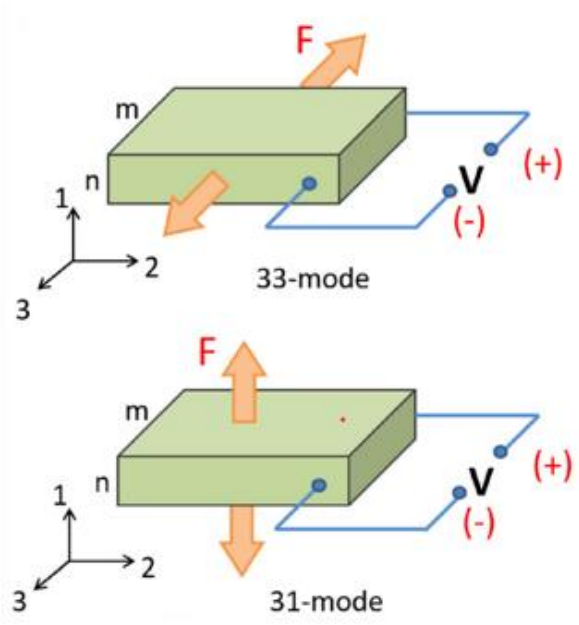

Figure 2.1. Cartesian coordinate system of a PVDF [62].

Piezoelectric materials exhibit two co-existing phenomenon which are; direct piezoelectric effect and indirect piezoelectric effect [59]. Direct piezoelectric effect is defined as the property causing non-centrosymmetric materials to produce an electric charge when a mechanical strain is applied. Indirect piezoelectric effect is the deformation of piezoelectric materials when electric current is passed through the material [63].

The performance of the piezoelectric harvester depends on mechanical-electrical conversion efficiency of the transducer [59]. The conversion efficiency can be calculated as in Equation (2):

$$E\% = \frac{Pout}{Pin} = \frac{V_p I_p}{Fv} \ , \tag{2}$$

where V_p is the voltage between the transducer's electrodes, I_p is the current flowing through the piezoelectric circuit, F is the external mechanical force and v is the speed of movement.

Some of the known advantages and disadvantages of piezoelectric harvesters can be summarized as in Table 2.4 [59].

Table 2.3. Advantages and disadvantages of piezoelectric harvesters.

Advantages	Disadvantages
High power and energy density	Harvested power require rectification
Made of a simple structure	Generate high voltage but very low current
Does not require external voltage source	Harvested power is low compared to different harvesters
Has good scalability	
Have high curie temperature	

2.5.1.1 Piezoelectric energy harvesting for WBANs

Considering that human motion generates high amplitude and low frequency voltage signals, PVDF is more appropriate for wearable applications where flexibility is essential. The harvester is easily implemented in shoes, bags, and clothing [61]. As

for mode of operation, most piezoelectric harvesters for wearable applications are based on 31-mode because this mode can effortlessly yield more considerable strain by lower pressures compared to 33-mode [64].

2.5.1.2 Analytical modeling of a piezoelectric biomorph harvester

The constitutive equation for a piezoelectric biomorph operated in 31-mode can be expressed as shown in Equation (3) below [65]:

$$T_1 = c_{11}S_1 - e_{31}^T E_3 \ , \tag{3a}$$

$$D_3 = e_{31}S_1 - e^S E_3 \ , \tag{3b}$$

where T_1 is the stress, S_1 is the strain, E_3 is the electric field intensity, D_3 is the electric displacement, c_{11} is the elastic compliance, e_{31} is the piezoelectric coefficient, e^s is the permittivity under constant or zero strain. To derive the analytical equations for the charge accumulated on the electrodes of a piezoelectric biomorph, a cartesian reference of a biomorph (piezo bender) is shown in Figure 2.2, where *L* is the beam length, *w* is the beam width, and *d* is the beam thickness.

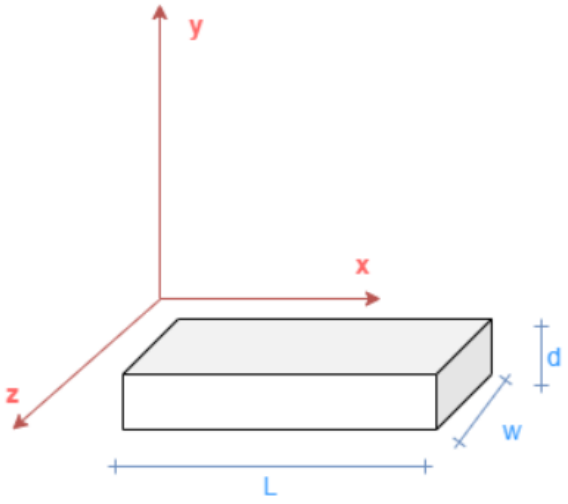

Figure 2.2. Cartesian reference of the Piezo Bender

Only forces applied in the y-direction are considered in this block. Therefore, to describe the kinematics, only the vertical displacement in the *y*-direction of the

center of gravity of each cross-section, *y(x)*, and the rotation around the *z*-axis of each cross-section, $\varphi_z(x)$ is specified. The piezoelectric material is polarized to bend only in the x-y plane. A strain field in a Euler-Bernoulli beam subject to bending is equal to:

$$S_{xx}(x,y) = -y\frac{d\phi_z}{dx}(x) \quad . \tag{4}$$

Where, $S_{xx}(x, y)$ is the strain function in the x-y plane, which is equal to the amount of vertical displacement in the y- direction times the derivative of the rotation around the z-axis per cross-section.

Because the electric field is constant between the positive and negative plates,

$$E_y = \frac{v}{d}. \tag{5}$$

With E_y denoting the electric field in the y direction, *v* the potential difference and *d* the thickness of the piezo beam.

Equation (3a) can be re-written as,

$$T_{xx} = s_{11}y\frac{d\phi_z}{dx}(x) - e_{31}\frac{v}{d} \quad . \tag{6}$$

The bending moment from the stress field is defined as:

$$M_z(x) = -\int yT_{xx}(x,y)dS = Ey^2\frac{d\phi}{dx}(x) + e_{31}\frac{v}{d}\int ydS \quad . \tag{7}$$

M_z is the bending moment in the z-direction. The remaining symbols in (7) are as defined previously.

Since the polarization of the material for $y = \left[-\frac{d}{2}, 0\right]$ is the opposite of the polarization for $y = \left[0, \frac{d}{2}\right]$, 31-mode piezoelectric stress-charge coupling coefficient changes sign, and the bending moment is defined as,

$$M_z(x) = \frac{E}{12}wd^3\frac{d\phi}{dx}(x) + wde_{31}v = EI\frac{d\phi_z}{dx}(x) + wde_{31}v \quad , \tag{8}$$

where $I = \frac{1}{12}wd^3$ is the second moment of area of the rectangular cross-section. The first term in Equation (8) is the standard equation of a beam subjected to bending. The second term is electromechanical coupling due to the presence of a voltage across the piezoelectric material. The induced voltage produces a uniform electrical bending moment along the beam.

Substituting Equation (4) to Equation (3b) results in:

$$D_y(x,y) = -e_{31}y\frac{d\phi}{dx}(x) + \frac{\varepsilon v}{d}\,. \tag{9}$$

The electric charge inside a volume is equal to the Gauss integral of the electric displacement[65]:

$$dq(x) = \oiint DydS = e_{31}\,dwdx\frac{d\phi_z}{dx} = e_{31}dwd\phi_z \quad . \tag{10}$$

The charge accumulated on the piezoelectric electrodes due to direct piezoelectric effect can therefore be defined as:

$$q = e_{31}dw(\phi_z(x2) - \phi_z(x1))\,. \tag{11}$$

2.5.2 Thermoelectric energy harvesting

Thermoelectric generator modules are becoming popular as a result of the growing need for energy-autonomous systems in the new era of WBANs, internet of things and other wireless sensor networks, where battery usage has proven insufficient [66]. A thermoelectric harvester/thermoelectric generator (TEG) is composed of N-pair of thermocouples containing p- and n-type semiconductors as depicted in Figure 2.3.

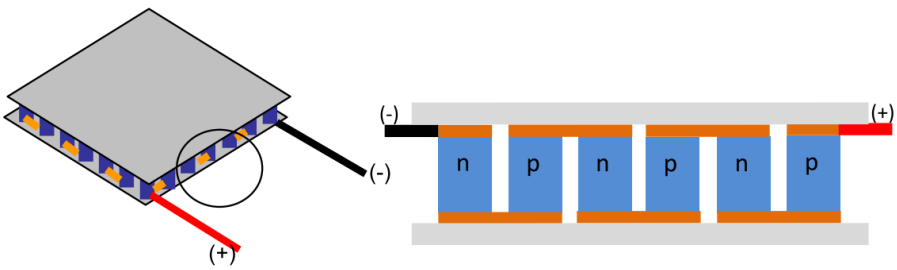

Figure 2.3. A thermoelectric module [66].

Thermocouples are connected thermally in parallel and electrically in series. These devices employ the Seebeck effect in a thermopile (many thermocouples) to convert temperature gradients to electricity [67], [68]. Seebeck effect is when two junctions of two different conducting materials produce a potential difference when maintained at different temperatures[67]. Figure 2.4 summarizes the electricity generation principle of a TEG.

Seebeck effect is directly proportional to temperature difference and the Seebeck coefficient of conducting materials as described in Equation (12):

$$V = \alpha \Delta T \,, \tag{12}$$

where α is the Seebeck coefficient and ΔT is the temperature gradient of the hot and cold junctions.

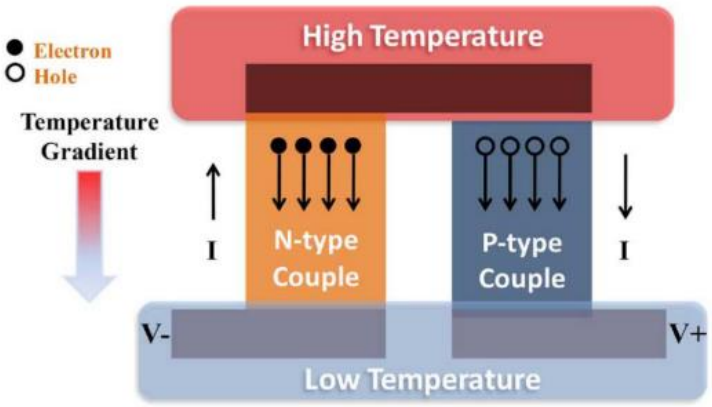

Figure 2.4. Working principle of a TEG

In a more general sense, a thermoelectric material is characterized using its figure of merit Z. This is a measure of how suitable the thermoelectric material is for power generation application. A good choice of thermoelectric material is one with a low electrical resistivity (ρ), high Seebeck coefficient (α) and a low thermal conductivity (λ). Equation (12) demonstrates the thermoelectric figure of merit [66]. Bismuth telluride Bi_2Te_3 is the most used thermoelectric material as seen from literature.

$$Z = \frac{\alpha^2}{\rho\lambda} \quad . \tag{13}$$

For accurate prediction of the energy harvested from a TEG, there are essential factors to note. First, the thermal resistance on the cold side is a major limiting factor due to forced convection, which results in limited heat dissipation from the module's cold side. As a result, the temperature of the cold side is not equal to ambient air temperature, contrary to many assumptions in the literature. Second, Joule heating, Thomson effect and the Peltier effect must be accounted for because they contribute to losses across the TEG module [68], as described below.

i) Peltier effect

When current flows between the hot and the cold junction, there is heat absorption or dissipation at the link of two conducting materials. This phenomenon is known as Peltier effect [69].

ii) Thomson effect

When an electric current passes through a circuit made of one material (homogeneous conductor), with a temperature gradient along its length, heat is either absorbed or dissipated depending on the direction of current. The described result is Thomson effect [70].

$$Q_t = -\mu_T \cdot I \cdot \frac{dT}{dx}, \tag{14}$$

where *Qt* is heat absorbed or dissipated, μ_T is the Thomson coefficient.

iii) Joule heating

Any material that has a non-trivial resistance dissipates heat when conducting electricity. This is known as Joule heating [71].

$$Q_J = I^2 R, \tag{15}$$

where Q_j is the heat absorbed, *I* is the current and R is the electrical resistance of the material.

The advantages of using TEGs for power generation include the fact that they are silent with no moving parts, reliable, and easily scalable.

2.5.2.1 Sustainability aspect of TEGs

Using waste heat and the ambient air to generate a temperature gradient for TEGs is cost-effective given that such heat is ubiquitously available [67]. Owing to the fact that 70% of world energy production is wasted through heat dissipation into the atmosphere [72], converting some of these heat into electricity is a positive effort towards environmental preservation.

2.5.2.2 Wearable thermoelectric generation

In wearable applications, the hot side of the TEG is in contact with the skin while the cold side faces the ambient environment [27]. Commercially available TEG modules for wearable applications have sizes ranging between 2-10 cm^3 [73]. Proposed modules in literature tend to vary in size depending on the intended application. For example, Pietryzk *et al.* in [68] presented a module that is 42 cm^3 in volume while Kanimba and Tian proposed a module that is 0.0125 cm^3 [74]. Both are for wearable applications.

The maximum theoretical conversion efficiency of TEGs can be expressed using Equation (16) [75]:

$$\eta_{max} = \frac{T_h}{T_c} \frac{\sqrt{1+Z\overline{T}}-1}{\sqrt{1+Z\overline{T}}+\frac{T_h}{Tc}} \quad , \tag{16}$$

where T_h is the hot side's temperature, T_c is the cold side temperature, zT is the average figure of merit.

2.5.2.3 Analytical modeling of thermoelectric harvester

Heat flow from the hot to cold junctions for N semiconductor thermocouples is expressed using Equation (17):

$$Q_h = N((\alpha_P - \alpha_N)IT_h + (\frac{k_p A_p}{L_p} + \frac{k_n A_n}{L_n})(T_h - T_c) - 0.5(\frac{\rho_p L_p}{A_p} + \frac{\rho_n L_n}{A_n})I^2) \ , \quad (17a)$$

$$Qc = N((\alpha_P - \alpha_N)IT_c + (\frac{k_p A_p}{L_p} + \frac{k_n A_n}{L_n})(T_h - T_c) + 0.5(\frac{\rho_p L_p}{A_p} + \frac{\rho_n L_n}{A_n})I^2) \ , \quad (17b)$$

Both *p* and *n*-type semiconductor legs can be manufactured with the same geometry and doped using the same alloys to reduce the manufacturing cost such that $L_p=L_n$, $A_p=A_n$, $\alpha_p=\alpha_n$, $\rho_{p=}\rho_{n,}$ $_{kp}=k_n$[74].

Power generated by the TEG transducer can be determined by obtaining the difference between the heat absorbed at the hot side and the heat rejected at the cold side[74].

2.5.2.4 Analytical modeling of TEG modules for WBANs

In wearable applications, Equations (17a-b) are equated to the body temperature, ambient temperature, and the thermal resistance of both the heat sink of the TEG and the skin, as demonstrated in Equations (18a-b):

$$\frac{T_{body} - T_h}{\phi_{skin}} = K(T_h - T_c) + SIT_h - 0.5I^2R = Q_h \ , \quad (18a)$$

$$\frac{T_c - T_{air}}{\phi_{heatSINK}} = K(T_h - T_c) + SIT_c + 0.5I^2R = Q_h \ , \quad (18b)$$

where T_{body}, T_{air}, φ_{skin}, $\varphi_{heatSINK}$, S, K, R are the temperature of the body, ambient temperature, thermal resistance of the skin, the thermal resistance of the heat sink, Seebeck coefficient of the module, thermal conductance of the module, the electrical resistance of the module, respectively. *K, S, R* and can be expanded as in equation (19-21):

$$K = \frac{A_s k FF}{L} \ , \quad (19)$$

$$S = N(\alpha_p - \alpha_n) \ , \quad (20)$$

$$R = \frac{4N^2\rho L + 8N^2 R_c}{A_s FF} \ . \quad (21)$$

FF in Equation 19 can be expanded as in (22):

$$FF = \frac{2NA_c}{A_s}, \quad (22)$$

where A_c is the cross-sectional area of each thermoelectric leg and A_s is the surface area of the TEG module. To simplify Equation (19), the leg length and the fill factor can be combined into a single factor B, where:

$$B = \frac{L}{FF} \quad . \quad (23)$$

Noting also that current,

$$\mathrm{I} = \frac{\mathrm{S(T_h - Tc)}}{1+\mathrm{x}}, \quad (24)$$

x being the ratio between load resistance and the module electrical resistance [68]. Equation (18), because of the above simplifications, becomes (25):

$$\frac{T_{body}-T_h}{\phi_{skin}} = Q_h = \frac{A_s k}{B}(T_h - T_c) + \frac{(\alpha_p-\alpha_n)^2 A_s (T_h-T_c)}{4B\rho(1+x)} T_h - \frac{A_s}{8B\rho}\left(\frac{(\alpha_p-\alpha_n)(T_h-T_c)}{1+x}\right)^2, \quad (25a)$$

$$\frac{T_c-T_{air}}{\phi_{heatSINK}} = Q_c = \frac{A_s k}{B}(T_h - T_c) + \frac{(\alpha_p-\alpha_n)^2 A_s (T_h-T_c)}{4B\rho(1+x)} T_c + \frac{A_s}{8B\rho}\left(\frac{(\alpha_p-\alpha_n)(T_h-T_c)}{1+x}\right)^2. \quad (25b)$$

2.6 System research in autonomous health-monitoring WBANs

EH for wearable health monitoring systems and WBANs has been studied extensively in recent years, with each study taking on a different approach. Süleyman *et al.* [19] did an overview of EH methods for wearable body area networks. [76] and [77] focused on the design of interface electronics for EH. Roy and Calhoun [2] presented a power management unit that harvests energy from either PV cells or TEG to power a biomedical load. Badri et al. [78] focused on dynamic slot allocation at different sensor nodes to maximize the lifetime in EH for wireless body sensor networks (WSN). Fan et al. [79] collected data to investigate usable power from EH based on various human activities and environmental data. Guo *et al.*[80] presented a paper on transmission scheduling in the wearable health monitoring system to optimize energy usage from the harvester to the loads.

As evident above, many studies on EH for wearable health monitoring devices and WBANs tend to concentrate on a single component/area of the system. While such studies are critical, optimizing an energy autonomous WBAN for cost, size, and performance requires that the behavior of all system components working collectively is studied to ensure that power generation, losses and delivery are properly balanced. In addition, there is a need for an analysis tool to facilitate in-depth understanding of various design trade-offs associated with the building blocks within WBAN nodes operating interactively in a particular system environment. In the literature, there has been some attempts to develop holistic systems or tools for understanding the power consumption and flow from generation to loads side of HMS. A tool kit developed by Tobola et al. in [31]was aimed at systems powered with batteries. In another study done by Taiyang et al., an autonomous flexible solar harvester based IoT connected WBAN was developed [81]. Dionisi et al. [82] also developed a fully autonomous solar based health monitoring system which is implemented on a T-shirt. Even though they make advances in the development of HMS, such studies still have some shortcoming as will be discussed in the following subsections. Section 2.7.1 to 2.7.3 describes the systems briefly and identify the existing gaps in literature for the development of fully autonomous health monitoring systems that explore a complete design space.

2.6.1 The Ultra-Low-Power Sensor Evaluation Kit

Tobola et al. [31] designed a three-part tool box for ultra-low power sensor evaluation reffered to as ULPSEK. The three parts include:

i. A modular sensor evaluation kit for development of ultra-low power health monitoring sensors;
ii. A miniturized wearable and code compatible sensor system with the same properties as development kit,
iii. A web based battery-runtime calculator for the ULPSEK based sensors.

The objective of ULPSEK is to optimize the power consumption within a health monitoring system. Different parts are discussed in further detail next.

i. ULPSEK for development (Figure 2.5) can evaluate the power consumption of different vital parameter sensors, processing units such as microcontrollers, radio modules and the circuit's power supply. The featured sensors include those that measure electrocardiography, Oxygen saturation, skin temperature, acceleration, and photoplethysmography (PPG). Both the hardware and software of ULPSEK are reported to be configurable to adjust to the monitoring conditions and environmental conditions.

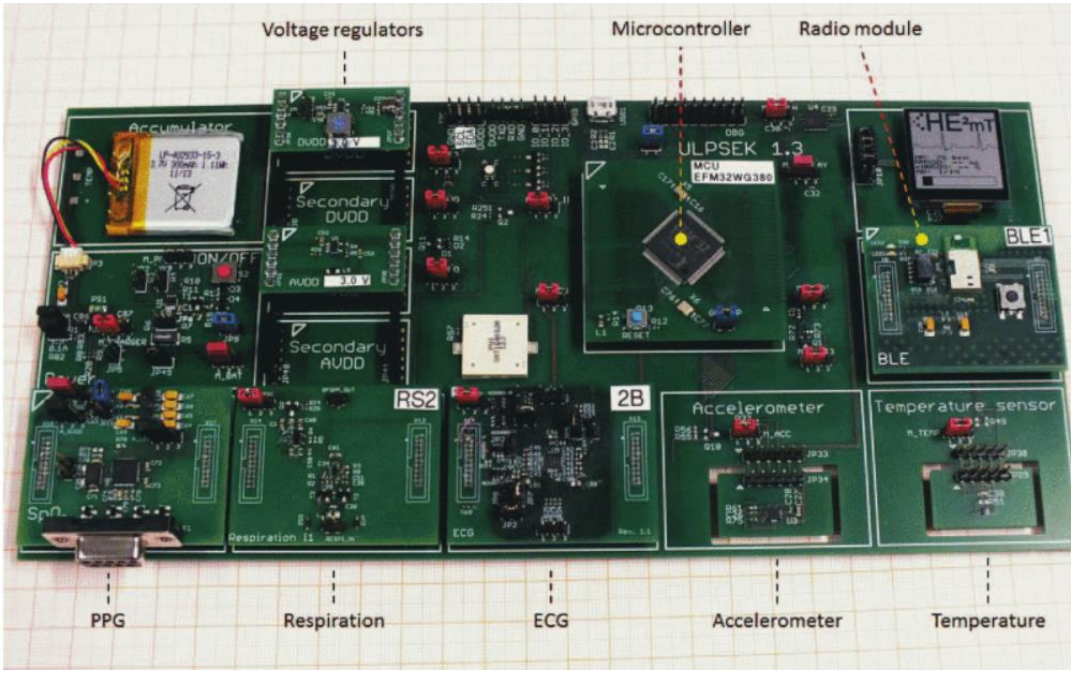

Figure 2.5. ULPSEK sensor evaluation kit for development [31].

ii. The miniaturized sensor system (Figure 2.6) is designed as a code compatible chest sensor belt with off-the shelf components such as 3.0 V linear voltage regulators TPS78230DRVT, microcontroller EFM32WG390F256, radio module PAN1721, ECG AD8232, inductive respiration, accelerometer MMA8452QT, temperature sensor TMP102 and TFT display LS013B7DH03 memory.

iii. ULPSEK's web-based battery runtime calculator enables designers to quickly understand how certain decisions and parameters affect the battery runtime. It is built as an interactive, web-based application based on, Java-Script, HTML, CSS Bootstrap and Knockout. The sensor system components such as the battery type, Voltage regulator, sensor modules and algorithm for important computation can be selected to calculate the overall runtime of the chosen battery type. Figure 2.7 shows a snippet of the energy model in use.

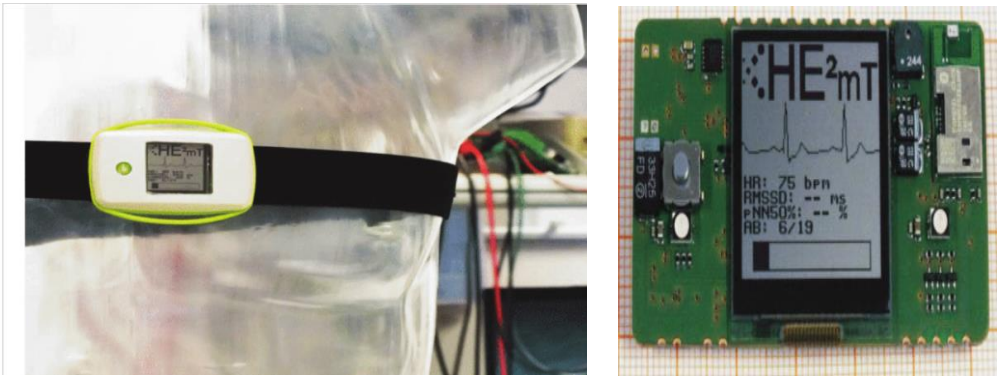

Figure 2.6. Miniaturized version of ULPSEK worn as a chest belt[6]

Summary		
Total average power consumption		704.1 µW
Battery runtime		1.1 months
Power supply properties		
Battery	CR2032 200 mAh	
Digital power supply	TPS78230 3.0 V	
Analog power supply	TPS78230 3.0 V	
System Voltage	3 V	
ECG properties		
ECG mode	Sampling 200 Sa/s	
ECG frontend	AD8232	549 µW
ECG sampling and QRS detector		278.8 µW

Figure 2.7. Battery runtime calculator from ulpsek.com

ULPSEK is a step in the right direction for investigating power consumption in ultra-low power health monitoring sensor systems. However, its focus on battery-based systems contrasts with the direction recent studies are taking of making health monitoring systems completely autonomous.

2.6.2 An Autonomous Wireless Body Area Network Implementation Towards IoT Connected Healthcare Applications

In [81], Tayiang et al. developed a health monitoring system, as depicted in Figure 2.8), based on a microcontroller as described in Chapter 2 Section 2.3.1. This wearable health monitoring sensor node is powered through solar harvesting and uses BLE as the communication standard thus enabling the implementation of a fully autonomous WBAN. The solar harvester is implemented with flexible photovoltaic panels for easy wearability and a maximum power point tracking (MPPT) module to harvest maximum power from the harvester. A buck-boost converter is used to regulate the harvested power, and the current from this converter is used to charge a supercapacitor.

The proposed system allows the deployment of multiple sensor nodes at different body parts of the user to measure the temperature, heart rate and any falling event. The implemented system size is 24cm^2 for each node, as shown in Figure 2.9. The BLE consumes 17.96 mA and 18.2 mA for receiving and sending data respectively. The temperature sensor, the pulse rate monitor, and the accelerometer consume 600 µA, 100 µA, 2 µA respectively.

All the sensors are based on ATmega 328 microcontroller whose features are attractive for this application due to its high performance, low power consumption and low cost. The supercapacitor (12.5 F), used as energy storage, takes about 25 minutes to charge on a sunny day and 115 minutes to do so on a cloudy day. When a user is wearing the proposed system, the experiments show that the system is fully

autonomous if the user spends some time outdoors and measures the required health signals.

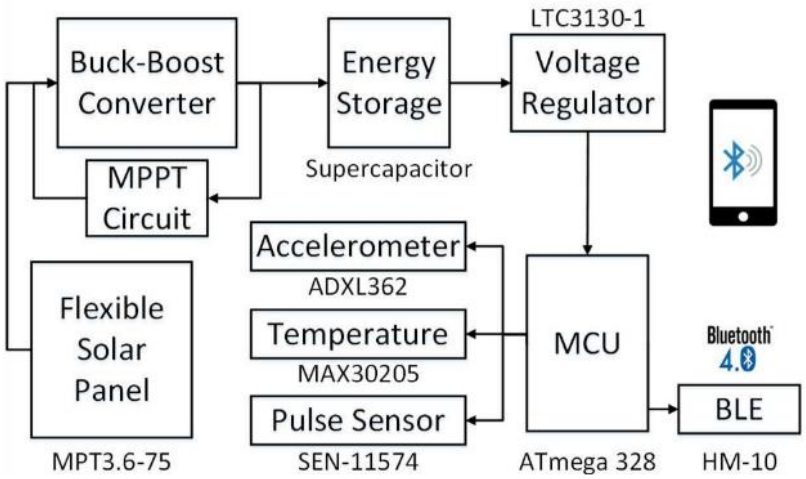

Figure 2.8. Taiyang et al.'s WBAN node block diagram [81]

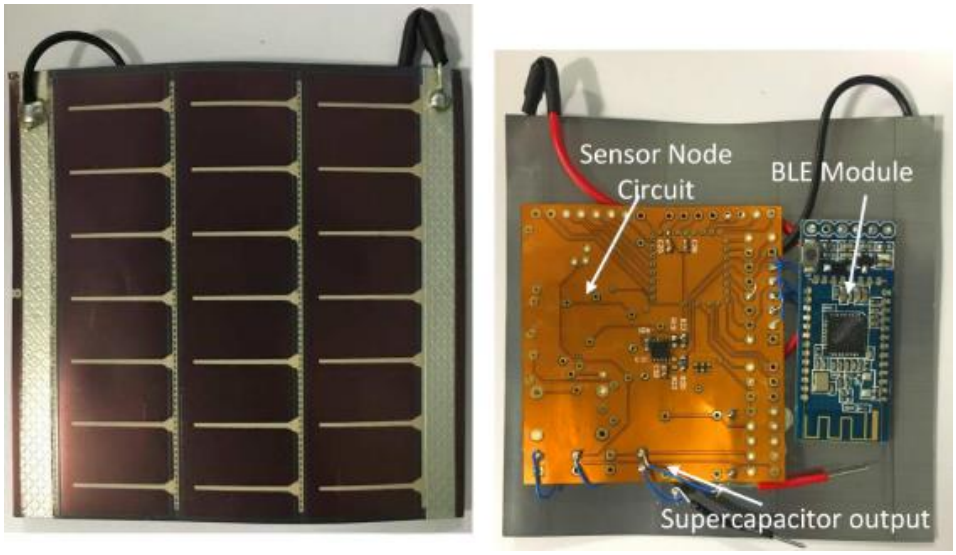

Figure 2.9. Implemented WBAN node [81]

In addition to the flexible solar harvester sensor node, Taiyang et al. also developed a smart phone application that is web-based for receiving the notification of the collected temperature, heart rate and acceleration data. This acts as the IoT gateway through which a doctor or a caregiver would receive the health information. Figure

2.10 shows the flow chart for the software at the sensor node, while the application of two sensor nodes are illustrated in Figure 2.11.

Even though Taiyang et al.'s system is self-powered, the solar power source limits its application to users who are able to spend time outdoors. In cases where the patient is bedridden, the system would not work due to the limited amount of power that can be harvested in an indoor setting. This greatly limits the flexibility of the system's application. In addition, the system does not self-power during a rainy, winter seasons with no sunshine or during the night. A harvester based on body movement and body heat does not suffer such intermittency because the human body heat is always available and activity for motion-based harvester can often be voluntarily induced, as part of a physiotherapy or therapeutic rehabilitation program.

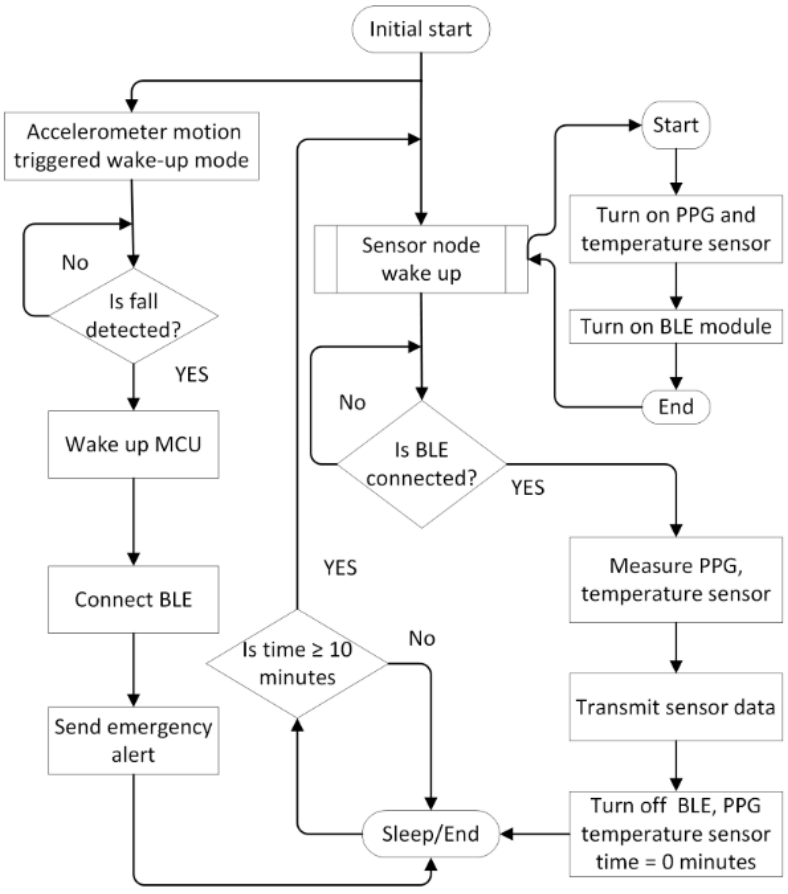

Figure 2.10. The software algorithm of the wearable sensor node [81]

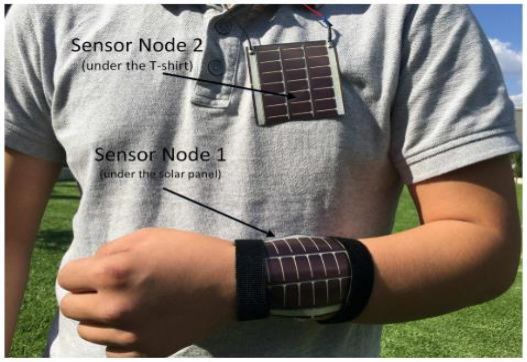

Figure 2.11. The system when in use with two sensor nodes [81]

2.6.3 Autonomous Wearable System for Vital Sign Measurement with Energy-Harvesting Module

Dionisi *et al.* [82] developed a batteryless, self-sustained wearable system for measuring heart rate, torso movement, and for measuring the respiration rate in a patient or any user. The autonomous system is based on the smart textile as described in Chapter 2 Section 2.3.2, with energy harvesting implemented for full autonomy. An autonomous T-shirt powered by a flexible solar panel applied directly on the T-shirt was used to measure health vitals. Figure 2.12 shows the block diagram of the system. The figure illustrates the cardiac activity module, the motion and tilt module, respiratory module, the power management circuit, a micro-controller, RF module, and the solar panel.

PT15-50 solar panel used in the system is 27 cm x 17 cm, weighing about 56.4 g. The overall size of the power electronics circuit board is 24.75 cm^2, and weighs 25g while the area covered by the cardiac electrodes is 49 cm^2. The systems are spread on the smart T shirt as shown in Figure 2.13. The system is evaluated under several lighting conditions to test its robustness, including indoor and outdoor with different weather conditions. The system employs duty cycling to reduce the power

consumption and has an average power consumption of 17 mW which allows continuous supply to the circuit board for powering all the loads in normal conditions. The energy stored in the supercapacitor can power the system for about 2 minutes in case of a short event of solar unavailability.

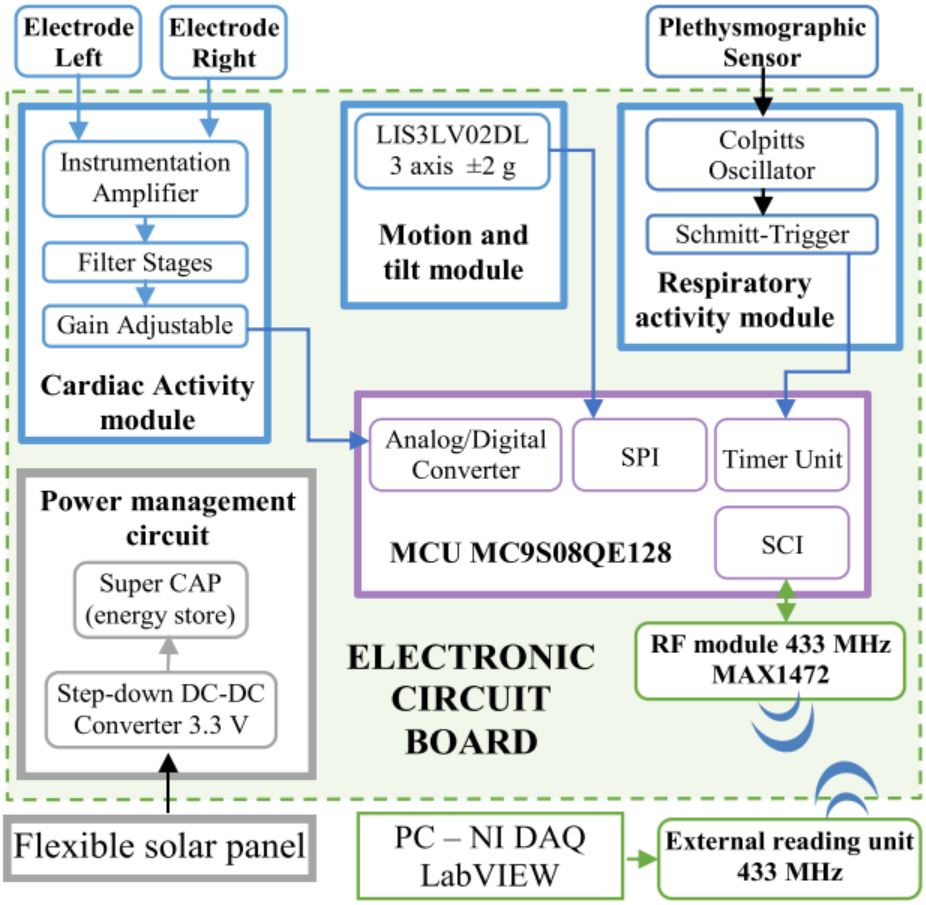

Figure 2.12. System architecture of the smart T-shirt [82]

The textile based autonomous health monitoring system developed by Dionisi is a good contribution towards replacing the unsustainable batteries with a renewable source of energy. This source is however dependent on the availability of the sun and cannot be used when the weather conditions are unfavorable. In addition, Dionisi's system is not a tool that can be used for design space exploration to make important design decisions that govern the energy consumption in an autonomous system.

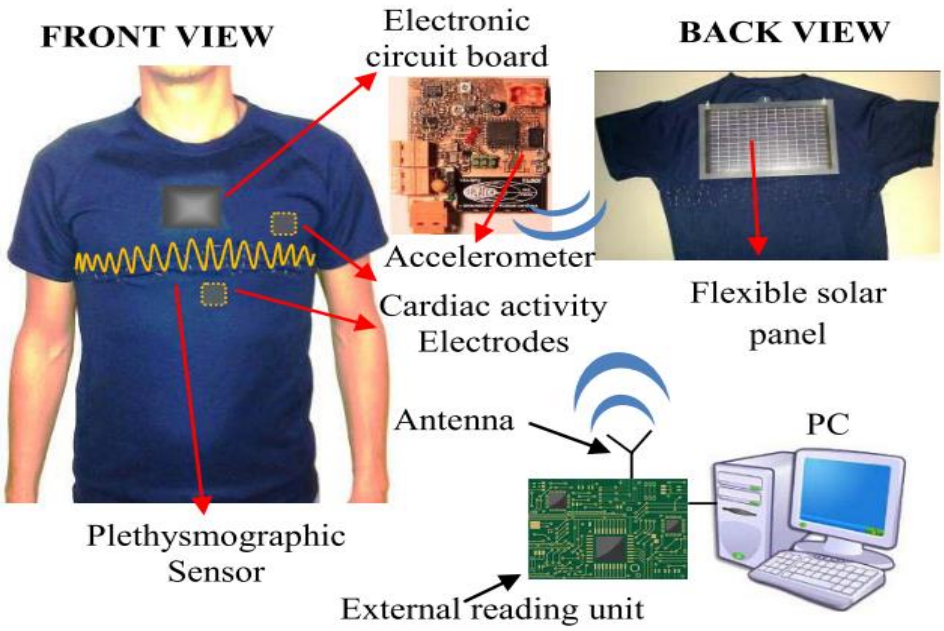

Figure 2.13. Dionisi et al.'s smart T-shirt powered by solar harvesting [82]

2.6.4 Implementation of Energy-Neutral Operation on Vibration Energy Harvesting WSN

Chamanian et al proposed in [83] proposed an innovative method to bridge the output power intermittency in vibration based harvester systems used to power WSN. The proposed system adjusts the duty-cycle by weighing the energy provided by the harvester and the required energy for each task in the WSN. The system is configured to sleep mode when there is no energy available for harvesting. The self-adaptive algorithm for altering the duty-cycle of the system depending on energy availability can be employed in WHMS with energy harvesting. Figure 2.5 shows the algorithm flow chart.

The proposed system solves the energy intermittency in vibration based harvesters but does not include detailed generation to load side modeling of these self-powered wireless body area networks.

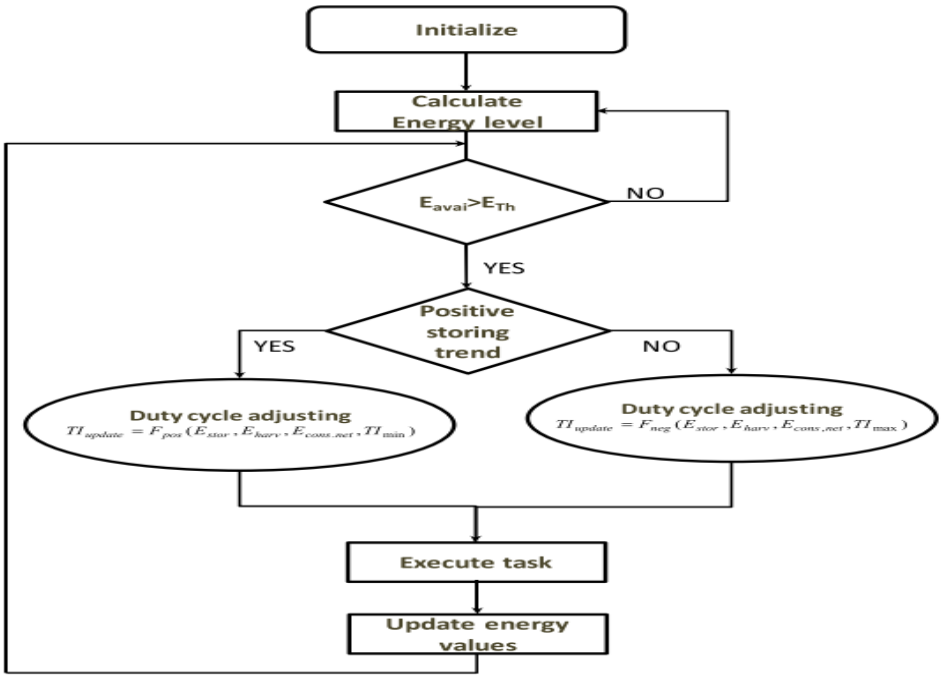

Figure 2.5. Flow chart of the self-adaptive algorithm for duty cycle adjustment[83]

Hence, the proposed work by Chamanian et al, can be included as part of system adjustments in the self-powered health monitoring systems in a more detailed tool as the one proposed in this thesis.

2.6.5 Efficient resource allocation in energy harvesting wireless networks

Ersoy developed an algorithm that employs energy harvesting prediction to predict the energy expected to arrive and hence scheduling operation of various power-hungry parts of a WBAN node such as the transceiver based on the systems energy profile. In this study, the schedule of load activity is determined, by assuming that the energy harvesting times and the corresponding harvested energy amounts are known at the beginning of each frame. This was done by formulating and solving a utility maximizing scheduling problem in a multiuser broadcast channel with an energy harvesting transmitter. Ersoy determined in her work the optimal power and time allocations to users between energy arrivals.

Table 2.4. Summary of literature review

System	Featured sensors	Energy source	Comments
ULPSEK By Tobola et al.	ECG, PPG, Temperature.	Batteries	Focused on battery powered systems.
Dionisi et al.	ADXL-345, Temperature, pulse rate,	Solar	Demonstrates self-powered WBANs i.e not a tool
Wu et al.	ADXL-345, Temperature, pulse rate,	Solar	Demonstrates self-powered WBANs i.e not a tool.
Ersoy	WSN	Solar	Algorithm for efficient energy scheduling. Not holistic.
Chamanian et al.	MicaZ mote	Electro-magnetic and Piezoelectric	Algorithm for duty-cycling in self powered WSN. Not holistic.
TEG powered ULPSEK	ECG, PPG, Temp-erature, Motion, pulse	TEG	Insufficient energy harvested.
HeMeS	Pulse rate, ECG, motion, Temperature	Piezoelectric and TEG	Unified model

In conclusion, there is no comprehensive system model available in the literature to investigate generation to consumption energy flow within a self powered WBAN which can be powered using a single or hybrid harvester, or a similar tool that can be used to investigates various design trade-offs in these autonomous systems depending on the environmental conditions and use case. This thesis contributes to the existing literature by proposing a Health Monitoring Energy System (HeMeS) tool that will fill the existing gap. The proposed system is implemented in Matlab/Simulink with a low level of complexity for quick analysis and design space exploration. So far there has not been any such implementation of energy modeling tools for WBANs in Matlab/Simulink.

CHAPTER 3

PROPOSED HeMeS TOOL

In this chapter the Health Monitoring Energy System (HeMeS) tool implementation is presented in detail. Initially, Analytical models of HeMeS system components are presented and then consolidated to form the complete Matlab/Simulink model of HeMeS. HeMeS core model is then converted into a user-friendly interface that can be used by various stakeholders such as sensor developers to study the energy flow in autonomous health monitoring systems. On the other hand, integrated circuit designers can also use HeMeS user interface to understand the possible sources of power loss in the system by doing an initial simulation of the behavior of the harvesters under various loading conditions and various system constraints. This chapter will also introduce various definitions of case studies that HeMeS will be used with to demonstrate the efficacy of the tool.

3.1 HeMeS system architecture

As previously introduced, HeMeS is a unified model with a hybrid thermal-vibrational energy harvester and a batteryless health monitoring WBAN node that shows the energy flow in an autonomous WBAN node and can be used to do design space exploration. A self-powered WBAN node is highly influenced by environmental constraints in which the system is employed, therefore all such factors must be included into HeMeS for an understanding of system behavior

Figure 3.1 shows the general concept of HeMeS system model and tool, with its overall inputs, outputs, and energy flow through components. The inputs include the environmental constraints such as temperature gradient used by the TEG for power generation, frequency, and displacement from vibrations during motion used for piezoelectric harvesting, maximum system dimensions, size constraints and system

efficiency. The load side constraints include the power requirements of the sensors, data processor and the communication channel. An energy balance within the system is sought for a predetermined period, typically set at 24 hours in the upcoming examples. If the system hits a zero balance, then the WBAN system node is considered autonomous.

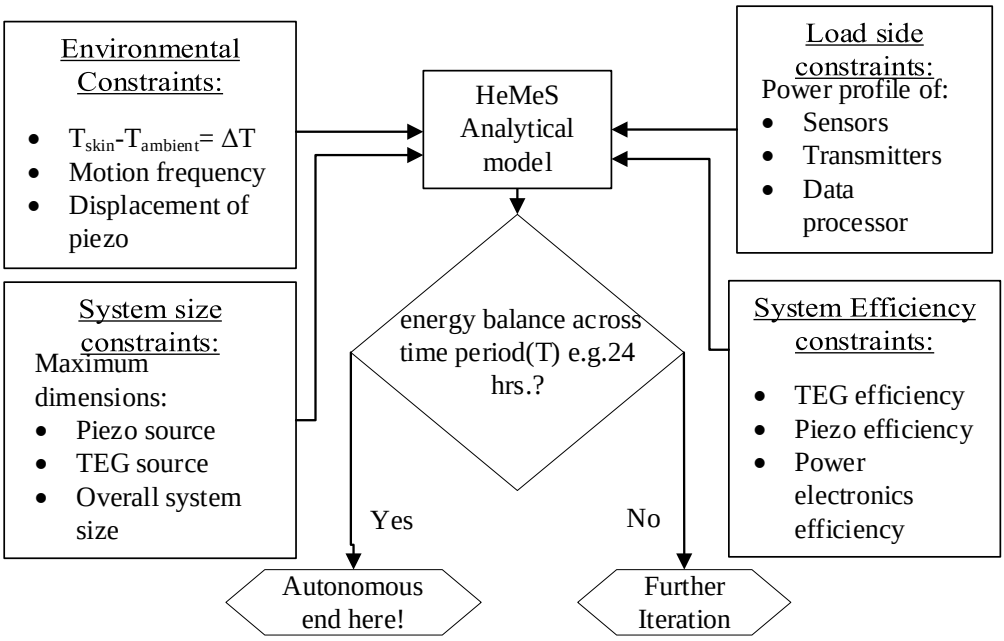

Figure 3.1. Proposed Health Monitoring Energy System (HeMeS) tool

3.2 Analytical modeling of HeMeS system components

Fig. 4.2 depicts a block diagram of HeMeS analytical model. It entails the power sources, interface electronics, the storage unit, and loads. The system is powered through thermal and vibrational EH. Thermal energy is harvested using a thermoelectric generator (TEG), while the vibration energy from human motion is harvested using a piezoelectric harvester. The thermoelectric harvester is selected because its output is not highly variable, has high power density and its suitable for indoor applications therefore the user has no obligation to spend time outdoors. The piezoelectric harvester also has high power density and can convert the low frequency vibrations into electricity.

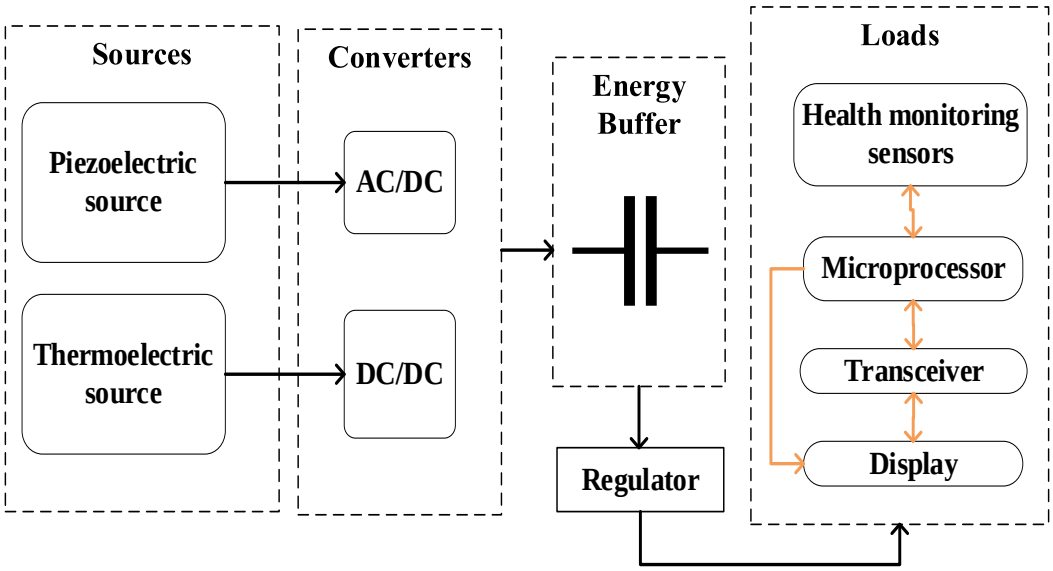

Figure 3.2. Block diagram of HeMeS analytical model

It is possible to extend the system scope to include electromagnetic harvesters for low-frequency vibrations and photovoltaic generators if system size constraints are relaxed.

WBAN loads require DC voltage. Therefore, the piezoelectric harvester is connected to an AC/DC converter and a filter to remove ripples from the rectified output. Similarly, the thermoelectric harvester is connected to a DC/DC boost converter to step up the low voltage from the TEG to the same level as the piezoelectric harvester. Once the two sources are conditioned to the same voltage level, they are combined into a single DC source whose output current is used to charge the storage capacitor. The storage capacitor acts as the energy buffer from which the WBAN loads are fed. A storage capacitor is chosen over a rechargeable battery because it has close to unlimited life cycles and therefore more durable compared to rechargeable batteries. A voltage regulator exists between the storage capacitor and the loads to ensure a steady output is maintained at the loads.

This system's loads comprise of a microcontroller with memory, a transceiver, a display, and health monitoring sensors, such as temperature, pressure, ECG and PPG

sensor, and an accelerometer. In the first revision of HeMeS, a system size of 10 cm^3 has been targeted for ease of integration in wearable health applications.

In the following subsections, the mathematical models of the system components are derived and afterwards implemented in Matlab/Simulink. Describing the system components using differential equations allow for easy conversion into Simulink blocks.

3.2.1 Power management unit

The HeMes tool is powered by a hybrid thermal-vibrational harvester. The derivation of induced charge in the piezoelectric harvester and induced voltage in the thermoelectric source for health monitoring WBANs was presented in chapter two.

3.2.2 Hybrid energy source

The piezoelectric source and thermoelectric source are conditioned to the same level and combined into a single DC source. The current from hybrid source is used to charge the energy buffer which is discharged by the loads.

3.2.2.1 Piezoelectric source

The theoretical working principles of a piezoelectric source was derived in 2.6.1 The charge accumulated between the positive and negative electrodes in a piezo bender was stated to be described as: $q = e_{31} \cdot d \cdot w \cdot (\Phi_Z(x_2) - \Phi(x_1))$.

From the above equation the amount of charge accumulated by the piezo bender is directly proportional to the piezoelectric coefficient(e_{31}), the thickness of the piezoelectric beam(d), the width of the beam(w) and the amount of displacement from initial position $\phi_z(x_2) - \phi_z(x_1)$.

Since the differential of the accumulated charge on the surface of the electrodes is the current flowing to the external impedance(Z), the amplitude of the current can be calculated as in (26) [84]

$$I = \omega q \tag{26}$$

Where ω is the frequency of the mechanical vibration of the piezoelectric biomorph.

3.2.2.2 Thermoelectric harvester

The heat flow equations between the hot and cold side of a TEG used in harvesting energy from the human body were also discussed in 2.6.2. Iteratively solving equations (25a-b) gives the actual temperature of the hot and cold side (T_h and T_c).

The voltage and output power of the TEG harvester can then be obtained by (27) and (28) respectively.

$$V=\frac{(S(T_h-T_c))x}{x+1} \quad , \tag{27}$$

$$P=IV=\frac{(S(T_h-T_c))^2x}{R(x+1)^2} \quad . \tag{28}$$

Where S is the seebeck coefficient, x is the ratio between the internal resistance of the harvester and the external load and R is the load resistance.

The outputs from both sources must be conditioned afterwards using various interface electronics.

3.2.3 Interface electronics

WBAN loads are dominantly powered using DC power [26]. Therefore, the harvested energy must be converted to a suitable form. AC voltage harvested from the piezoelectric harvester must be rectified and conditioned using a buck converter.

A typical rectifier circuit is normally made of diodes that allow current flow in only one direction. These diodes are however not suitable for low power energy harvesting due to their high forward voltages (0.6V) that significantly reduce the power conversion efficiency[21]. In literature, there exists active rectifiers made of Mosfets that are highly efficient and preferable for energy harvesting due their low on-voltage losses. For example, Herbawi et al. presented An Ultra-Low-Power Active AC-DC CMOS Converter for Sub-1V Integrated Energy Harvesting Applications. This active rectifier can rectify input AC signals with amplitudes in the range of 0.5-1.2 V with a maximum conversion efficiency of 94%[85]. Ciftci et al. also presented a low-profile and autonomous piezoelectric energy harvesting system consisting of an extraction rectifier[21]

HeMes is a system level model with high level of abstraction; therefore, a simple rectifier is implemented using an If statement pseudocode, which works as follows:

If Vpiezo > 0

Output = Vpiezo

Else if Vpiezo < 0

Output = -1 · Vpiezo

After obtaining the fully rectified lossless output, an efficiency factor based on literature is added to the model for accuracy purposes.

Similarly, the DC output of the thermoelectric harvester must be stepped up to the level needed for the intermediate storage capacitor. A small TEG module requires a suitable boost converter capable of operating with low input voltage levels as efficiently as possible.

Both boost and buck converters used in the HeMeS tool are modeled based on power conversion efficiency as presented in equation (29) [86]. Similarly, the DC output of

the thermoelectric harvester must be stepped up to the level needed for the intermediate storage capacitor.

$$I_{out\_converter}=\frac{\eta \cdot P_{harvester}}{V_{sc}} \quad , \tag{29}$$

where $I_{out\_converter}$, η, $P_{harvester}$, V_{sc} are output current, efficiency, harvester output power, and storage capacitor voltage (converter output voltage), respectively. The converter efficiency parameters account for the conversion losses.

3.2.4 Intermediate storage Unit

Accumulated current from both the TEG boost converter and the piezoelectric buck converter is used to charge a supercapacitor. The stored energy is then used to supply the load of the health monitoring system. An equivalent circuit for the Supercapacitor in figure 4.3 is represented using mathematical equations as shown in (30-33):

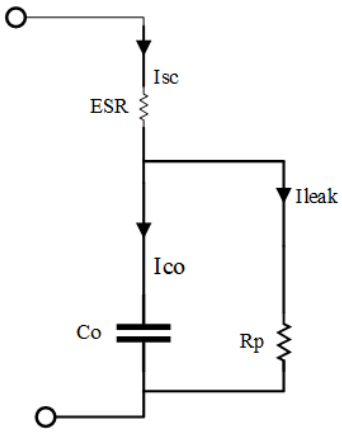

Figure 3.3. Equivalent Circuit of a supercapacitor[87]

$$V_{sc}=V_c+V_{ESR} \quad , \tag{30}$$

$$V_C=\frac{1}{C}\int I_C(t)\,dt+V_{c0} \quad , \tag{31}$$

$$V_{ESR}=I_{charge}\cdot ESR \quad , \tag{32}$$

$$I_C = I_{charge} - I_{leak} - I_{discharge} \quad . \tag{33}$$

V_{sc}, V_c, ESR, and I_c, I_{leak}, are supercapacitor voltage, capacitor voltage, electrical series resistance, capacitor current and the leakage current from the capacitor.

3.2.5 Loads

Loads are modeled based on their average total current consumption, which discharges the storage capacitor. HeMeS allows user-friendly entry of different activity levels and estimated durations of these activity levels for each load device to facilitate the calculation of total average current.

3.3 Implementation of HeMeS

The analytical models presented in Section 3.1.1are used to represent WBAN component Matlab/Simulink models within the HeMeS tool at the required system abstraction level.

3.3.1 Piezoelectric energy generator

A piezo bender from the Simscape library in Matlab is used to model the piezoelectric harvester as shown in Figure 3.3. To parametrize the piezo bender for wearable applications, T220-H4BR-1305XB, a commercial piezo bender, was chosen because it meets the required properties in terms of size and material flexibility for WBAN application. Its parameters are presented in Table 3.1.

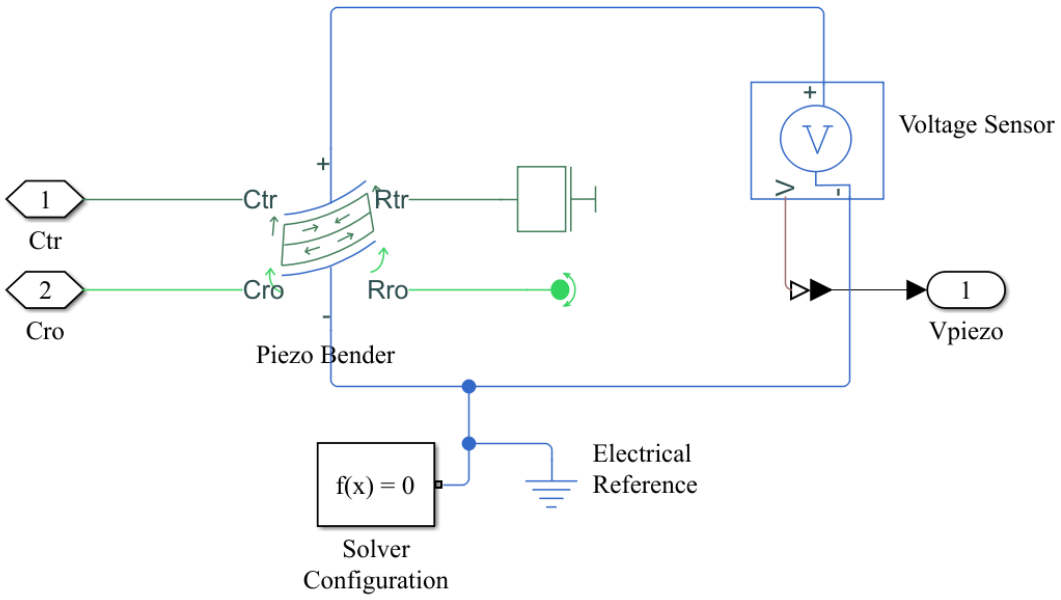

Figure 3.4. Piezo bender from Simscape library

Table 3.1. Datasheet parameters for T220-H4BR-1305XB [88]

Parameter	**Value**
Length (l)	31.7 mm
Width (w)	12.7 mm
Thickness (d)	0.51 mm
Mass (m)	1.6 g
Rated Voltage (V_{rated})	60 V
Free deflection at rated voltage (y_{free})	0.25 mm
Blocking force at rated voltage (F_{block})	0.28 N
Capacitance (Cpiezo)	24 nF

T220-H4BR-1305XB's parameters are used to calculate the fundamental material parameters of the piezo bender as in equations (34-36):

$$e_{31}=\frac{2lF_{block}}{3dwV_{rated}} \quad , \tag{34}$$

$$E=\frac{4F_{block}l^3}{y_{free}d^3w} \quad , \tag{35}$$

$$\varepsilon=\frac{d}{lw}\left(C_{piezo}+\frac{4F_{block}y_{free}}{V_{rated}^2}\right) \quad . \tag{36}$$

The first resonance frequency of the piezo bender can also be calculated using equation (21):

$$2\pi f_0=1.855^2\sqrt{\frac{EI}{ml^3}} \quad . \tag{37}$$

Upon calculation, the fundamental material parameters are obtained as outlined in Table 3.2.

The parameters are plugged into the model to calculate the amount of charge accumulated within the piezo bender. A voltage sensor connected across the piezo bender measures the induced voltage of the piezo bender, as depicted in Figure 3.3

Table 3.2. Fundamental material parameters

Fundamental Parameter	**Value from calculation**
Piezoelectric stress coefficient (e_{31})	15.275 C/m^2
Young's Modulus (E)	$8.5514*10^{10}$ N/m^2
Dielectric constant (Ɛ)	$1.28932*10^{-7}$ F/m
First resonance frequency(f_0)	52.8 Hz

The voltage output of a piezoelectric module is alternating in nature. Therefore, the vibration source is modeled using a sine wave whose frequency mirrors the vibration

frequency from human motion. The vibration source is then connected to the piezo bender. In addition to the voltage, the current I_p (shown in figure 3.2) through the piezoelectric capacitor is calculated using equation (38) [89]: The generated piezoelectric power can be predicted using (39)

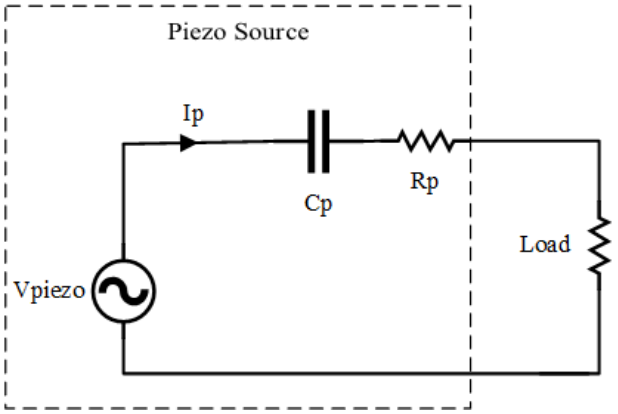

Figure 3.5. Electrical Equivalent circuit of the piezoelectric harvester

$$I_p = C_p \frac{dV_p}{dt} \quad (38)$$

$$P_{piezo} = V_{piezo} \cdot I_p \quad (39)$$

With all the necessary parameters obtained, the values are plugged into the piezo bender model in Matlab.

3.3.2 Thermoelectric generator

TEG datasheet parameters presented in table 3.3. are plugged into equation (25a-b) [90] to find the hot and cold side temperatures of the thermoelectric module from iterations in Matlab. Equations (27-28) are then converted into a Simulink model with a Matlab function to calculate the voltage and power induced by the TEG as illustrated in figure 3.5.

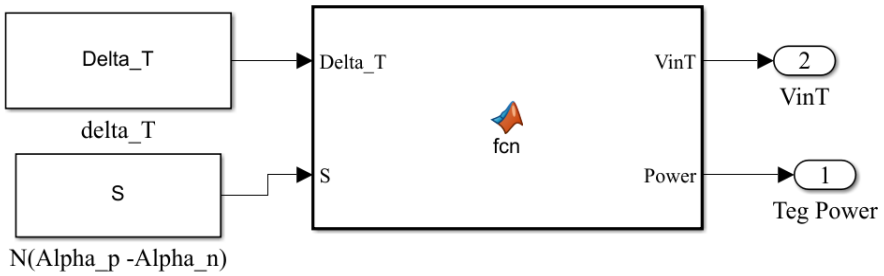

Figure 3.6. Simulink Model of the TEG

Table 3.3. Parameters used to model TEG in Matlab / Simulink [68],[91]

Description	Symbol	Value
The Surface area of the TEG	A_s	0.0016 m^2
Thickness of the module	t	5.1e-3 m
Thermoelectric material thermal conductivity	k	1.820 W/mK
Seebeck coefficient of the P-type leg	α_p	186e-6 V/K
Seebeck coefficient of the n-type leg	α_n	-186e-6 V/K
Electrical resistivity of the thermoelectric material	ρ	7.226e-6 Ωm
Temperature of the body	T_{body}	310 K
Thermal resistance of the skin	φ_{skin}	3.218 K/W
The thermal resistance of the heat sink	$\varphi_{heatSINK}$	21.74 K/W
Ratio of $R_{load:}$ R_{TEG}	x	1
Length/Fill factor	B	0.0336
No of leg pairs	N	199

3.3.3 Interface electronics

Simulink blocks are used to implement the rectifier pseudocode in 3.1.1.2. A low pass filter from Simulink library is also added to remove any ripples in the rectified output as shown in figure 3.7

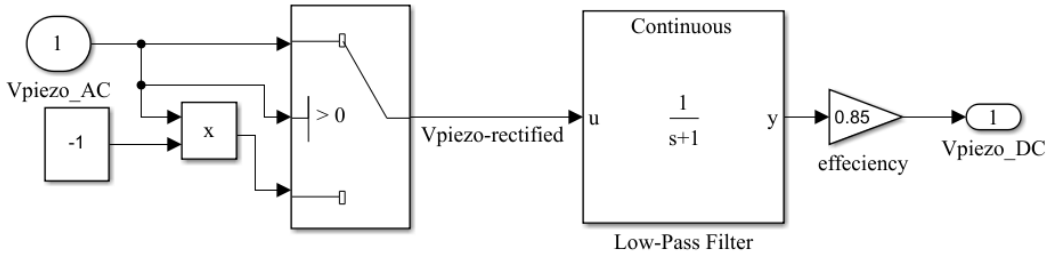

Figure 3.7. Simplified rectifier and filter for Piezo harvester

After conversion into a DC output, a buck converter is also implemented using a Matlab function to step down the voltage if the Vout from the piezoelectric generator rises above the required 3.3 V. The rectifier, the filter, and the buck converter are all implemented based on Linear Technology's harvester IC. LTC-3588 has an inbuilt bridge rectifier, a filter circuit, and a high-efficiency filter buck converter. The complete model of the piezoelectric harvester is shown in Figure 3.8

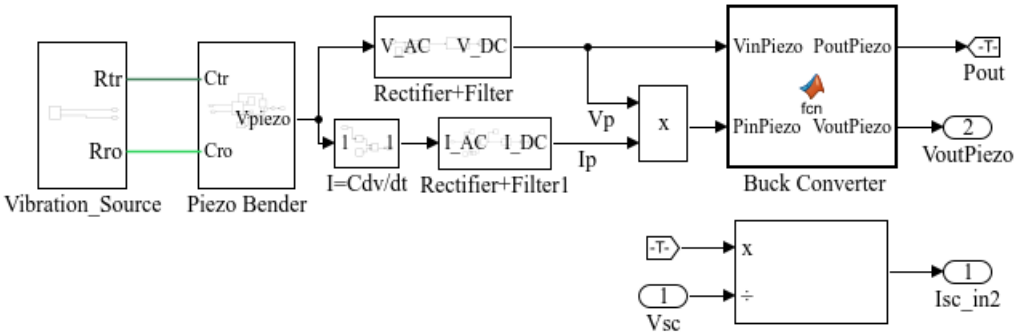

Figure 3.8. Complete Piezoelectric harvester Simulink model

The magnitude of the voltage harvested from the TEG is relatively low compared to that of the piezoelectric harvester. Since both sources are programmed to operate

simultaneously, the TEG voltage is boosted to the same level as the piezoelectric voltage (3.3V). The TEG DC/DC converter is modeled based on the TI-BQ25504 harvester IC. A Matlab function is used to model the boost converter following the energy efficiency modeling approach discussed in (29). The overall system for the thermoelectric generator is depicted in figure 3.9.

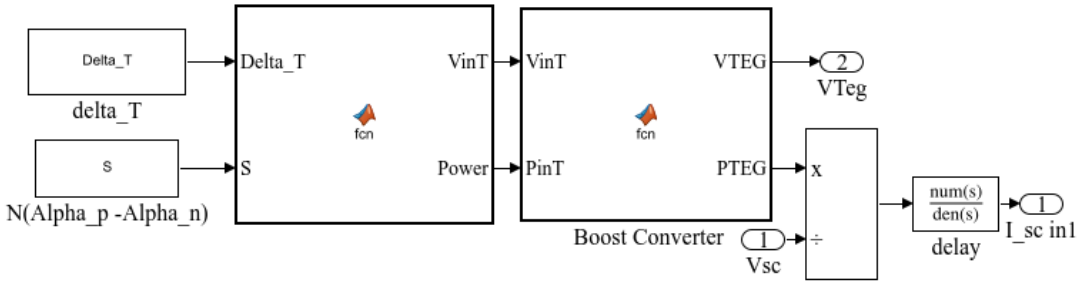

Figure 3.9. Complete thermoelectric harvester module

3.3.4 Intermediate energy storage

Equations (30-33) are converted to the equivalent Simulink model shown in Figure 3.10. A datasheet of a commercially available Supercapacitor is used to obtain the values of the equivalent series resistance (ESR), leakage current, and the rated capacitance[92]. The PB-5R0V104-R 100 mF from Eaton was chosen in this application.

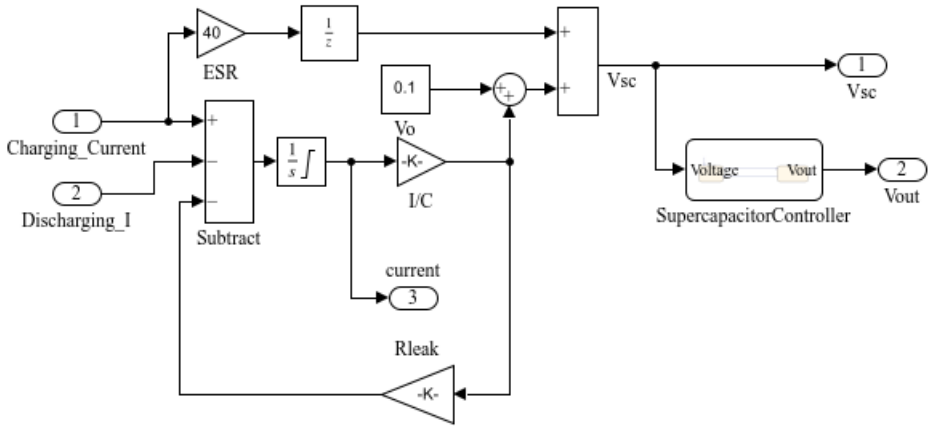

Figure 3.10. Supercapacitor Simulink model

3.3.5 Simulink Model of the voltage regulator

A voltage regulator which is designed based on conversion efficiency is also incorporated into HeMes. To calculate the actual current discharging the supercapacitor. The Simulink model shown in Figure 3.11 is used. This model mimics the operation of a voltage regulator.

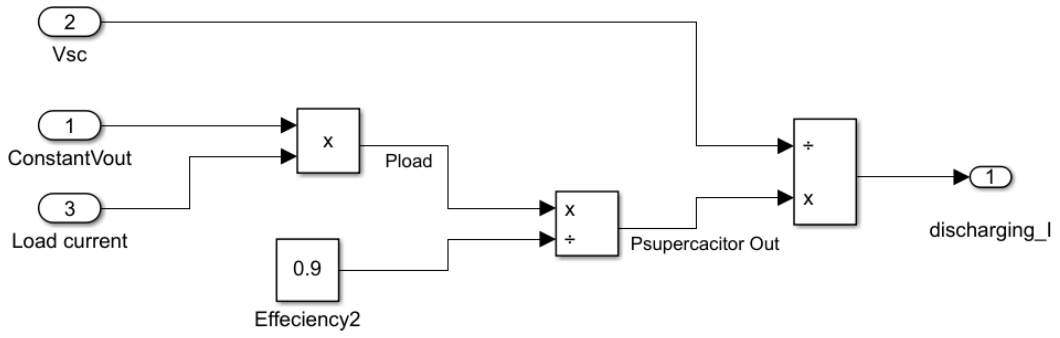

Figure 3.11. Simulink model of the voltage regulator

3.3.6 Loads

For HeMeS, the loading conditions are those that are compatible with the energy capacity of the harvester system. Therefore, each load is activated and consumes current only when sufficient energy is accumulated. Power saving practices such as transmission scheduling are employed to manage the power-hungry portions of the load.

Health monitoring sensors featured in the tool include; EPIC Ultra High Impedance Electrocardiogram(ECG) sensor[93], a temperature sensor, a pulse rate sensor, and a 3-axis accelerometer motion sensor. These health monitoring sensors whose functions were defined in chapter two are selected as part of the health sensors used with HeMeS. However other health sensors can also be included depending on the requirement of the user. Depending on the selected health sensors selected by the

user, the application areas can vary. However, it is crucial that the selected health monitoring sensor can be powered by the harvested energy from the load.

A 32-bit MCU Arm®-based Cortex®-M3 [94] micro-controller is selected for signal processing and conditioning and an low-power BLE is incorporated for communication that consumes 60 µA when in low power mode. BLE was discussed in detail in Section 2.4. The following subsections briefly discuss the loads.

3.3.6.1 Ultra- low power 32-bit Arm Cortex M3

The 32-bit Arm Cortex M3 microcontroller was selected for this application due to its desirable features for this application. The microcontroller's ultra-low power platform operates with voltages between 1.65 to 3.6 V power supply. During standby mode, the micro-controller consumes 290 nA with 3 wake up pins. The microcontroller takes up to 8 µs to wake up from standby mode. The current consumption during run mode is 195 µA/MHz. When in stop mode with 16 wakeup lines, the controller consumes 560 nA. When in low power mode the processor consumes 60 µA.

3.3.6.2 EPIC Ultra High Impedance ECG Sensor

The PS25251 is an ultra-high impedance solid state ECG (electrocardiograph) sensor. It can be used as a dry contact ECG sensor without the need for potentially dangerous low impedance circuits across the heart. It is best suited for non-critical patient monitoring, lifestyle sports and health products. Can be used for long-term and remote monitoring

It requires a current of 2.5 mA when active and 10 nA when in deep sleep mode, with a supply voltage ranging between 2.5-5.5 V

3.3.6.3 ADXL345- 3 Axis Accelerometer

The ADXL345 is a small, thin, low power, three-axis accelerometer with high resolution (13-bit) measurement up to factor in all g-ranges, up to ±16 g. The ADXL345 is well suited for mobile device applications. It measures the static acceleration of gravity in tilt-sensing applications, as well as dynamic acceleration resulting from inactivity sensing. It can also be used to detect a fall. ADXL 345 requires a voltage supply of 1.8 V- 3.6 V and occupies a volume of 15 mm^3.

Finally the pulse rate sensor [95] and the temperature sensor[94] consumes 30 µA and 100 µA respectively during active mode. In addition to active power, the pulse rate sensor also consumes 10 µA during idle mode.

3.4 HeMeS integration for full system and scenario analysis

To develop HeMeS, various energy harvesting methods that are compatible with WBANs have been studied in detail. In addition, mathematical models for the power electronics used in power conditioning have been studied to allow for temporary storage of the harvested energy on a capacitor/supercapacitor. A sensor node with updated requirements from literature studies has then been incorporated into the system using a user-friendly table. All the mathematical models are then converted into the equivalent Matlab/Simulink model and combined to form HeMeS. The harvested power is used to supply the WBAN node.

Figure 3.12 shows the full HeMeS Simulink model. For the system to rely on the low harvested energy, various energy saving techniques have been employed. The system components are put to sleep and only awakened when required, as was discussed in previous chapters. Additionally, in the piezoelectric source, the vibrations generated by human body movement are of frequencies less than 8 Hz [29], [55]. Thus, frequency up-conversion (FUC) can be employed to ensure a reasonable amount of energy is harvested [96][55]. Frequency up-conversion has

therefore been integrated as an option for HeMeS. The frequency up-conversion method introduced by Halim *et al.* in [96] is opted for in HeMeS. Its operation involves a metal ball of about 4.6g that mechanically and consecutively impacts two flexible piezoelectric-attached sidewalls when shaken. Each impact allows the sidewall to transfer impulsive force to the piezoelectric loaded mass and causes voltage generation by the piezoelectric effect.

The target system size for the thermal-vibrational powered sensor node has been initially set to 10 cm^3. This size will allow for easy integration for wearable application.

A user interface of HeMeS has been created for easy application. Input side constraints such as temperature gradient on the TEG mask, and a vibration frequency to the piezoelectric source, system size constraints and efficiency values of system components are entered by the user. Additionally, the current requirement of the WBAN node is also user prompted. Figures 3.13 to 3.16 show how the user interacts with HeMes. Once the user has entered all the input side and load side constraints, HeMeS tool automatically checks for system autonomy in the node.

To detect instantaneous power autonomy, a flag is included which outputs logic 1 when the system can self-sustain and 0 when the system does not have enough power to supply the load. The flag compares the supply current to discharging current using a logical operator.

This tool is used to study the power and energy flow from generation side to the load side and allows a quick analysis of various design tradeoffs as will be outlined in Chapter 4. In Figure 3.1 a conceptual diagram od HeMeS was introduced, The diagram included various system constraints. These constraints directly impact the behavior of the autonomous system. Section 3.5 defines these use case scenarios.

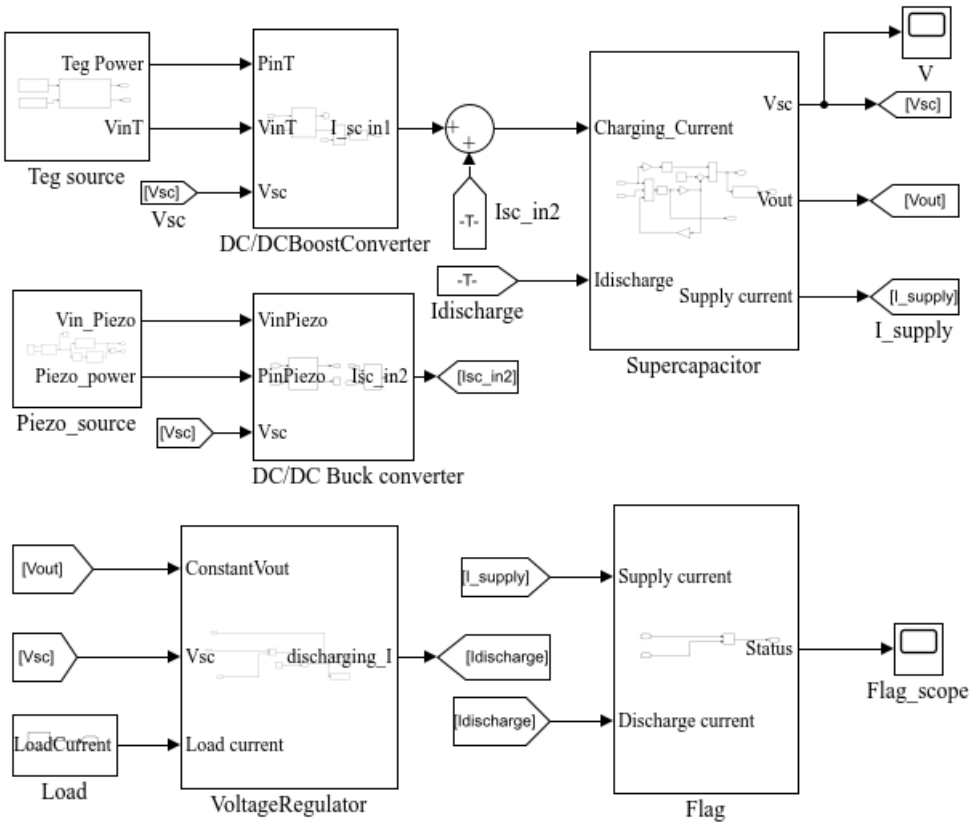

Figure 3.12. Complete Simulink model of HeMeS

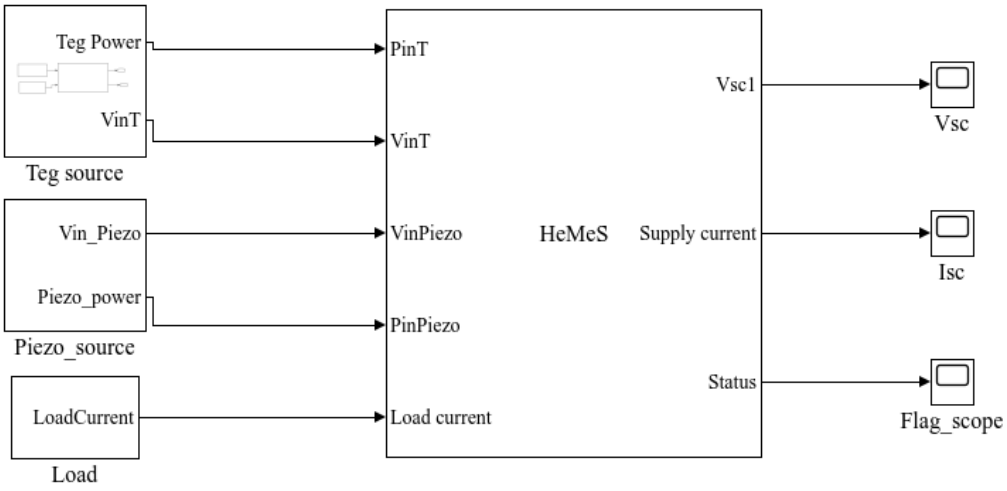

Figure 3.13. HeMeS User Interface

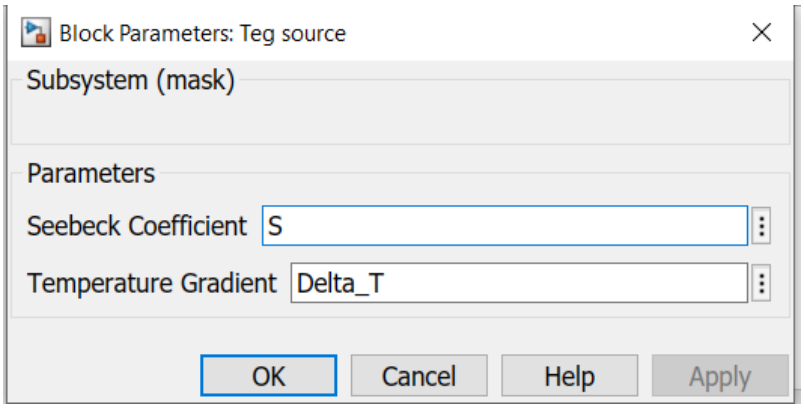

Figure 3.14. Temperature gradient Input

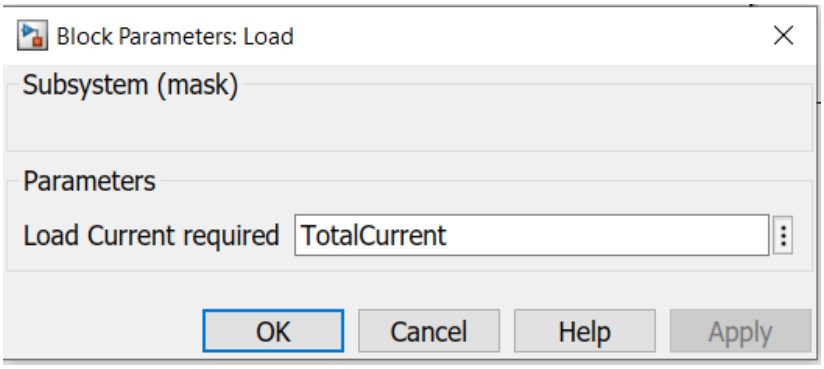

Figure 3.15. Load input

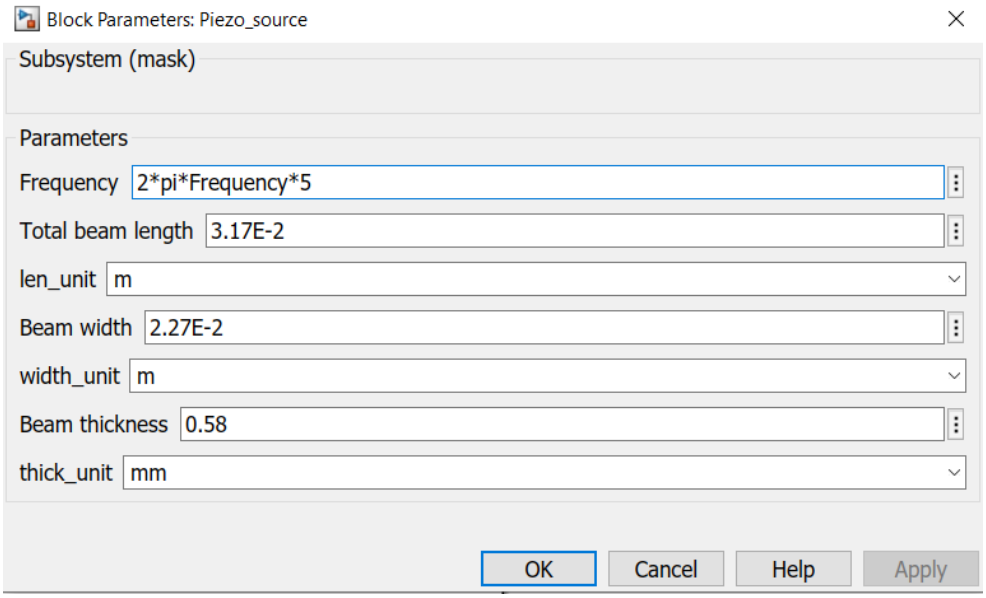

Figure 3.16. Piezo source Input

3.5 Use case definitions (Design space exploration methodology)

This subsection defines various scenarios for simulation using Matlab to identify the behavior of the system under different environmental constraints, for a period of 24 hours. HeMeS was tested with various types of patients including non-critical patients, nursing home patients and hospitalized patients to determine the minimum activity level and environmental constrains for autonomous operation, the maximum load activity level for autonomous operation and the minimum system size for autonomous operation.

The system is defined to be autonomous when the average power generated from the sources can sustain the loads and account for all the intra-system and inter-system losses, over a defined period (T) e.g., 24 hours. The system is tested with different types of patients, under variable environmental and load side conditions. At each instant a zero balance must be attained or else the system is iterated until a fully autonomous condition is achieved.

3.5.1 Non-critical patient

A non-critical patient in this case can be defined as a patient who is relatively mobile and can go through day-to-day activities without any physical hardship. Such a user can use a WBAN node to continuously monitor bio signals for an early detection of abnormalities. According to Demir et al.[19], continuous patient monitoring of health signals is becoming the new de facto to help reduce the ever increasing health care costs by determining any abnormal conditions before they develop into chronic diseases that are difficult to treat. Patients in this category can be very active during jogging exercises with a piezoelectric frequency of up to 4 Hz and with generated power depending on level of strain[96].

3.5.2 Nursing home patient

According to Georgie and Jeannes [97], elderly people living in nursing homes require close attention to monitor their health vitals because chronic conditions such as heart diseases and diabetes are quite common at their age. In addition, physical activity is also greatly reduced during this period in a person's life in general. To enhance independence among the elderly, Stefanos et al.[98] recommend the use of health monitoring sensors for continuous health monitoring to allow for early detection of any abnormalities and to monitor motion for fall detection. HeMeS tool was deployed for a scenario when such an elderly is using the tool. As described in both [97] and [98], nursing home patients (in most cases the elderly people) have lower activity levels. Therefore, it follows that the vibrations from their motion occur at even lower frequencies compared to other younger people.

3.5.3 Hospitalized patient

A hospitalized patient in this case is defined as one that is bedridden an in no position to move. Therefore, the design space exploration of this patient will mainly be influenced by the amount of harvestable power from the TEG.

3.5.4 Load activity constrained analysis to determine minimum user activity and environmental constraints-method

To determine the minimum level activity of each patient type and their environmental constraints for autonomous operations, the default load activity presented in Table 3.6, and the system size are kept constant, and the level of activity of the patient and environmental constraints are varied starting with the default conditions presented in Table 3.4. The figures shown in the table are derived from hourly data in literature [98], [99] showing the daily activity profile of both young adults and elderly patients coupled with the corresponding frequency of human

motion in [101]. In this table, the second column of the table the default level of activity for each patient is defined. These frequencies of motion are translated into how active a patient needs to be over 24 hours for autonomous operation. The third column shows the default temperature gradient required for thermoelectric harvesting sufficient. Each patient type exhibits different levels of activity depending on their capability. The ideal scenarios for 24-hour period autonomous operations are determined from iterations by steadily altering the default cases until a zero balance is attained.

Table 3.4. Default patient activity level and environmental conditions

Patient Type	**Avg. freq. of motion (over 24 hrs.)**	**Avg ΔT (over 24 hrs.)**
Non-critical	1.27 Hz	14.21 ℃
Nursing home patient (e.g.,elderly)	1 Hz	14.52 ℃
Hospitalized patient	-	15.02 ℃

3.5.5 User activity, and environmental conditions constrained analysis, to determine maximum load activity-method

The system includes various power consumption reduction techniques in the loads such as duty cycling, transmission scheduling and active and idle power modes to minimize system's overall power consumption. Loads are therefore only activated at intervals when needed to reduce power consumption in the node. In [102], Ersoy developed an algorithm that employs energy harvesting prediction to predict the energy expected to arrive and hence scheduling operation of various power hungry parts of a WBAN node such as the transceiver based on the systems energy profile. In this study, the schedule of load activity is determined, by assuming that the energy harvesting times and the corresponding harvested energy amounts are known at the beginning of each frame. This can optimize the activity level of each WBAN node.

In another study done in [83], Chamanian et al. developed an energy neutral WSN implemented using a MicaZ mote as the WSN and powered through a two vibration-

based harvesters. The node achieves energy-neutral operation by self-adjusting its duty-cycle depending on the available energy from the harvester. When no energy is available for harvesting, the proposed system goes to sleep mode. This study shows that the BLE transceiver operation protocol in HeMeS can also be adapted to availability of power and data and setting the tranceiver to idle mode unitl another episode experienced. Future versions of HeMeS can include these algorithms for further optimization in the system. In the first revision of HeMeS, to determine the maximum active time for each load component during a 24-hour period, for each patient type, the system is iterated with different percentages of activity in the loads for optimization. The default load activity shown in Table 3.5 is used as the starting point of the study. Table 3.5 is prepared following the recommendations in [23] showing how activity levels in WBAN nodes can be adjusted to minimize power consumption in the system. The activity levels are then adjusted steadily until an autonomous point is reached for each patient.

Table 3.5. Default load activity

Module	**Origin**	**State**	**%Time**	**Supply current**
MCU Arm®-based Cortex®-M3	Infineon	Active	5%	60 µA
		Idle	95%	2 µA
Ultra-low power BLE	On Semi.	Rx	2%	3.2 mA
		Tx	2%	3.3 mA
		Idle	96%	10 µA
Temperature sensor	Bosch Sensortec	Active	100%	3 µA
ADXL 345	Analog Devices	Active	100%	30 µA
Pulse rate sensor	Bosch Sensortec	Active	10%	100 µA
		Idle	90%	1 µA
EPIC ECG Sensor	Plessey Semi.	Active	3%	2.5 mA
		Idle	97%	10 nA

3.5.6 User and load activity constrained analysis to determine size-method

When movement, temperature, and WBAN node loads are fixed, a minimum system size for autonomous operation can be determined by doing a system sweep for various patient types. The size of the system includes the volume of constituent components but is mostly defined by the energy harvesters because the other components are a few millimeters in size. Additionally, the power generators i.e., the TEG and piezo components are the main determinants of whether the system operates autonomously since they provide system energy

Their sizes are a great determinant of how much energy is harvested from the system. Because the thermoelectric generator produces a considerable amount of power, its initially selected size was assumed optimal to keep the system within the required range for wearable application. The piezoelectric source on the hand can be adjusted to harvest more power in the system. Table 3.6 presents the power harvester sizes in volume.

Table 3.6. System size

Description	**Component**	**Volume**
TEG source	TEG-126 LDT	8.16 cm^3
Piezo source	T220-H4BR-1305XB	0.2053 cm^3
Overall system size	HeMeS	10 cm^3

CHAPTER 4

DESIGN SPACE EXPLORATION USING HeMeS-FINDINGS

This chapter demonstrates the results of using HeMeS under various scenarios to demonstrate the utility of the tool to achieve design conversion.

In the following subsections, minimum user activity, maximum load activity and minimum system size for autonomous operation will be respectively targeted for analysis, with the rest of the fixed system parameters used as constraints as was introduced in chapter 3. The objective is to explore the design space of a hybrid powered WBAN node to identify system capability under different conditions. To begin, the minimum required energy for autonomous operation in a WBAN node is determined over 24 hours. It must be noted however that the amount of energy required is variable depending on the load activity of each scenario. After determining this threshold, the system will be iterated using various patient types to determine the autonomous pass mark of each of those patient categories. Sections 4.1 to 4.3 contain the detailed results of each analysis. For each study, the system is tested with and without FUC. The advantage of using FUC as will be observed is the higher output power from the piezoelectric source which as a result offers more support to the TEG. It must be noted however that when the system uses FUC, an additional piezoelectric beam is required which impacts the overall system size. Patient scenarios with extreme size constraints may opt for cases without FUC and employ only a single piezoelectric harvester.

4.1 Load activity constrained analysis to determine minimum user activity-results

In this scenario, ideal environmental factors under which WBAN node operates autonomously is determined using HeMeS. The default scenarios were defined in the last section of Chapter 3.

A minimum patient activity set (for piezoelectric generation) and minimum temperature gradient set (for thermoelectric generation) are determined for the system to operate autonomously, when the system is used by different types of patients. From the study, it is understood that there is no unique solution to the system problem. Energy balance may be achieved through a variety of patient activity (and room temperature) profiles during different hours of the day. Therefore, in seeking a solution for a particular user activity profile, parameters were varied as little as possible from typical patient environment profiles published in the literature.

Patient activities in this category are classified as either maximum, medium, minimum or no activity. When the patient has maximum activity, it means that the patient is under some light aerobics with vibration frequencies of up to 4 Hz for non-critical patient and 2 Hz from nursing home patients. When there is medium movement, it is translated as the patient conducting some light errands that involve movement but not as high as those during light aerobics. In this case, the frequency of motion is about 2.5 Hz and 1.5 Hz for non-critical patient and nursing home patient respectively. When the patients exhibit minimum movement the frequency of motion of about 2 Hz is registered for the non-critical patient. The nursing home patient only records medium movement and minimum movement. These activity levels are adjusted depending on the defined system conditions. The activities can be spread over 24 hours depending on the preference of the patient. As long as the minimum average activity level has been met, the patient can stay idle as desired. The average of the activity level is what determines the autonomous operation of the system.

4.1.1 Non-critical patient with FUC enabled

An example of the minimum activity level for autonomous operation in a 24-hour period for a non-critical patient whose bio signals are monitored using HeMeS is presented in Table 4.2. The minimum average frequency of motion of the patient for the whole day should be 1.27 Hz and the temperature of the body and ambient air should be 36.92 ºC and 22.71 ºC respectively on average.

When the mentioned environmental conditions are met, the system operates autonomously and monitors the biosignals as necessary. It can be concluded that because the system employs FUC, the system operates autonomously using low average levels of activity because the raw movement frequencies are boosted by the system to higher levels for more output power.

4.1.2 Non-critical patient with monitored biosignals and FUC disabled

Unlike in 4.1.1 above, when the system does not employ FUC, and the low frequencies are used in the piezo source directly, a higher level of activity is expected in such a patient for system's autonomy. This is due to the previously stated low vibration frequencies from human motion. Hence within the 24-hour period, it is observed from iteration that the patient average frequency of motion should be 2.04 Hz for autonomous operation. In addition, a minimum temperature gradient of 14.87 ºC is required for the thermoelectric source to produce enough power to support the piezo source and hence the overall hybrid system. Table 4.3 presents the activity profile of such a patient. From this table we conclude that the minimum physical activity of the user must be significantly higher as opposed to the case in 4.1.1 to support the same load conditions, due to non-existent frequency up conversion. The average frequency of motion in this category must increase by 0.77 Hz from the FUC enabled case. The average temperature gradient over 24 hours must also increase by 0.66 ºC so that enough power would be harvested from the system for autonomous operation. Figure 4.1 and 4.2 summarizes the comparison between the level of

activities for the patient for both FUC enabled and FUC disabled cases and change in ambient temperature for the FUC and non FUC cases respectively for a non-critical patient with monitored biosignals.

Table 4.1. HeMeS 24-hour activity profile and environmental constraints with FUC

Time (24hours)	Activity	Temp body(°C)	Temp ambient(°C)	Frequency of motion (Hz)
7:00:00 AM	Max	37.5	25	3
8:00:00 AM	Max	37.5	25	3
9:00:00 AM	Medium	37	25	2.5
10:00:00 AM	Medium	37	25	2.5
11:00:00 AM	Medium	37	25	2.5
12:00:00 PM	Min	36.5	25	2
1:00:00 PM	Min	36.5	25	2
2:00:00 PM	Min	36.5	25	2
3:00:00 PM	Min	36.5	25	2
4:00:00 PM	Min	36.5	25	2
5:00:00 PM	Medium	37	25	2.5
6:00:00 PM	Medium	37	25	2.5
7:00:00 PM	Min	36.5	25	2
8:00:00 PM	No	37	20	0
9:00:00 PM	No	37	20	0
10:00:00 PM	No	37	20	0
11:00:00 PM	No	37	20	0
12:00:00 AM	No	37	20	0
1:00:00 AM	No	37	20	0
2:00:00 AM	No	37	20	0
3:00:00 AM	No	37	20	0
4:00:00 AM	No	37	20	0
5:00:00 AM	No	37	20	0
6:00:00 AM	No	37	20	0
Whole day	Average activity	**36.92**	**22.71**	**1.27**

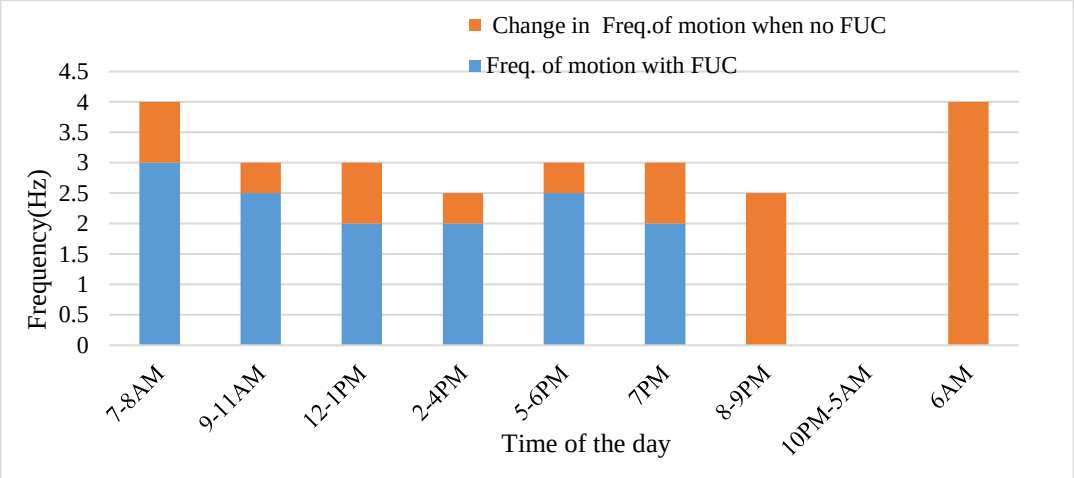

Figure 4.1. Noncritical patient activity level for FUC enabled and FUC disabled

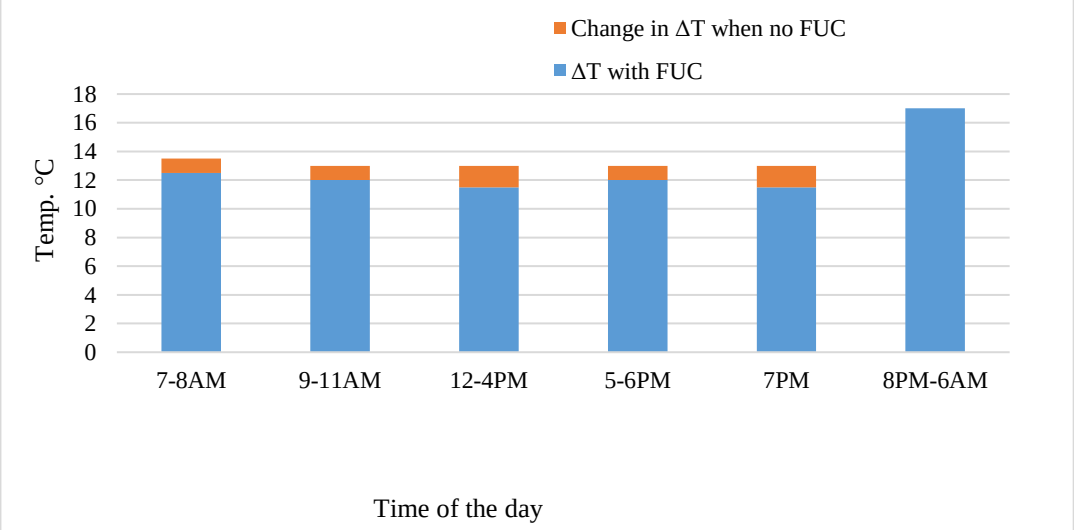

Figure 4.2. ΔT for non-critical patient for FUC enabled and FUC disabled cases.

4.1.3 Nursing home patient with FUC enabled

The activity profile for an elderly person for HeMeS is shown in Table 4.4. In a 24-hour window, a minimum average of 1 Hz is expected along with a minimum temperature gradient of 14.52 ºC for a WBAN node to be autonomous. Compared to

Table 4.2, the decrease in patient activity has been compensated through temperature gradient, assuming a small adjustment to room temperature was acceptable.

Table 4.2. HeMeS 24-hour activity profile and environmental constraints without FUC

Time (24hours)	**Activity**	**Tbody(°C)**	**Tair(°C)**	**Frequency of motion (Hz)**
7:00:00 AM	Max	37.5	24	4
8:00:00 AM	Max	37.5	24	4
9:00:00 AM	Medium	37	24	3
10:00:00 AM	Medium	37	24	3
11:00:00 AM	Medium	37	24	3
12:00:00 PM	Medium	37	24	3
1:00:00 PM	Medium	37	24	3
2:00:00 PM	Min	37	24	2.5
3:00:00 PM	Min	37	24	2.5
4:00:00 PM	Min	37	24	2.5
5:00:00 PM	Medium	37	24	3
6:00:00 PM	Medium	37	24	3
7:00:00 PM	Medium	37	24	3
8:00:00 PM	Min	37	20	2.5
9:00:00 PM	Min	37	20	2.5
10:00:00 PM	No movement	37	20	0
11:00:00 PM	No movement	37	20	0
12:00:00 AM	No movement	37	20	0
1:00:00 AM	No movement	37	20	0
2:00:00 AM	No movement	37	20	0
3:00:00 AM	No movement	37	20	0
4:00:00 AM	No movement	37	20	0
5:00:00 AM	No movement	37	20	0
6:00:00 AM	Max	37	20	4
Whole day	Average activity	**37.04**	**22.17**	**2.04**

Table 4.3. 24-hour activity profile and environmental constraints of a nursing home patient with FUC

Time (24hours)	Activity	Tbody	Tair	Frequency of motion
7:00:00 AM	Medium	37.5	24.5	2
8:00:00 AM	Medium	37.5	24.5	2
9:00:00 AM	Medium	37	24.5	2
10:00:00 AM	Medium	37	24.5	2
11:00:00 AM	Medium	37	24.5	2
12:00:00 PM	Min	37	24.5	1.5
1:00:00 PM	Min	37	24.5	1.5
2:00:00 PM	Min	37	24.5	1.5
3:00:00 PM	Min	37	24.5	1.5
4:00:00 PM	Min	37	24.5	1.5
5:00:00 PM	min	37	24.5	1.5
6:00:00 PM	min	37	24.5	1.5
7:00:00 PM	Min	37	24.5	1.5
8:00:00 PM	No	37	20	0
9:00:00 PM	No	37	20	0
10:00:00 PM	No	37	20	0
11:00:00 PM	No	37	20	0
12:00:00 AM	No	37	20	0
1:00:00 AM	No	37	20	0
2:00:00 AM	No	37	20	0
3:00:00 AM	No	37	20	0
4:00:00 AM	No	37	20	0
5:00:00 AM	No	37	20	0
6:00:00 AM	Medium	37.5	20	2
Whole day	Average activity	**37.06**	**22.44**	**1**

4.1.4 Nursing home patient with FUC disabled

In this case, there is a need for a higher level of activity unlike in the FUC case. The 24-hour average frequency of motion and temperature gradients expected from the elderly monitored patients is presented in Table 4.5. The minimum average

frequency expected is 1.54 Hz with a minimum temperature gradient of 15 ºC. The level of increase in activity when FUC is disabled is 0.54 Hz and a general increase in the temperature gradient by 0.48 ºC.

Figure 4.3 and 4.4 summarizes the comparison between the level of activities for the patient for both FUC enabled and FUC disabled cases and change in ambient temperature for the FUC and non FUC cases respectively for a nursing home patient with monitored biosignals.

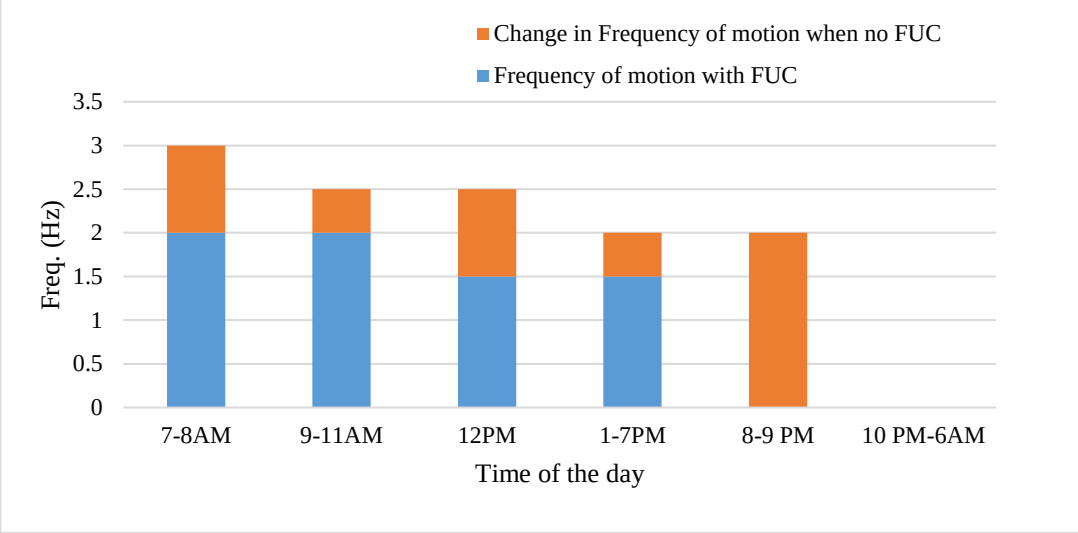

Figure 4.3. Nursing home patient activity level for FUC enabled and FUC disabled

4.1.5 Hospitalized patient

The hospitalized patient in this case is assumed to be in no position to move. The primary source of power in HeMeS in this case is therefore exclusively the TEG source. The patient activity profile is presented in Table 4.6. For this case, enabling or disabling frequency up conversion clearly does not make a difference in the system. A minimum temperature gradient of 15.02 °C is required for the system to continue operating autonomously without movement. Figure 4.5 shows the temperature gradient adjustments over a 24-hour period for autonomous operation.

Table 4.4. 24-hour activity profile and environmental constraints of a nursing home patient using HeMeS without FUC

Time (24hours)	**Activity**	**Tbody**	**Tair**	**Frequency of motion**
7:00:00 AM	Max	37.5	24	3
8:00:00 AM	Max	37.5	24	3
9:00:00 AM	Medium	37	24	2.5
10:00:00 AM	Medium	37	24	2.5
11:00:00 AM	Medium	37	24	2.5
12:00:00 PM	Medium	37	24	2.5
1:00:00 PM	Min	37	24	2
2:00:00 PM	Min	37	24	2
3:00:00 PM	Min	37	24	2
4:00:00 PM	Min	37	24	2
5:00:00 PM	Min	37	24	2
6:00:00 PM	Min	37	24	2
7:00:00 PM	Min	37	24	2
8:00:00 PM	Min	37	20	2
9:00:00 PM	Min	37	20	2
10:00:00 PM	No	37	20	0
11:00:00 PM	No	37	20	0
12:00:00 AM	No	37	20	0
1:00:00 AM	No	37	20	0
2:00:00 AM	No	37	20	0
3:00:00 AM	No	37	20	0
4:00:00 AM	No	37	20	0
5:00:00 AM	No	37	20	0
6:00:00 AM	Max	37	19	0
whole day	average of activity	**37.04**	**22.13**	**1.54**

Notably, the temperature gradients for this patient type are higher than the nursing home and non-critical patient cases. This is because the TEG solely supports the WBAN node.

Table 4.7 summarizes the output powers for each case and each source when there is FUC and no FUC and in the hospitalized case.

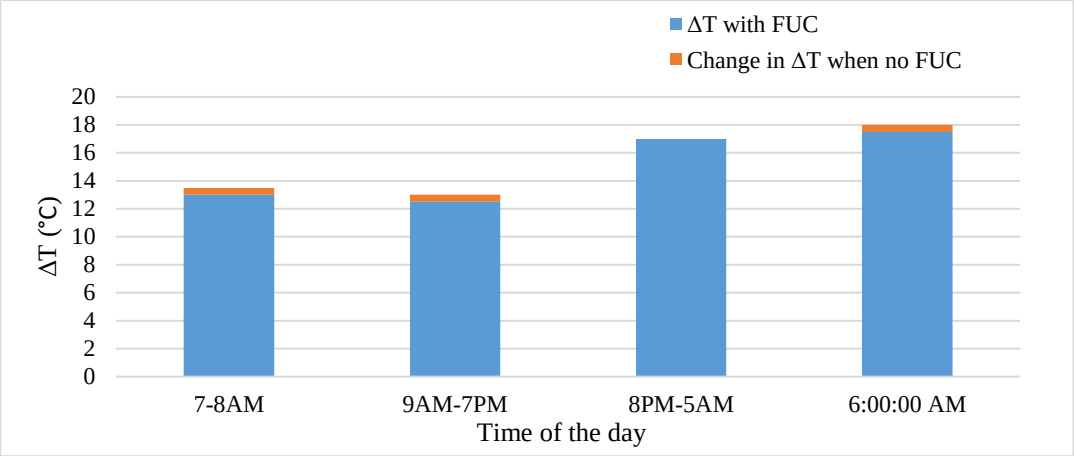

Figure 4.4. ΔT for nursing home patient for FUC enabled and FUC disabled cases

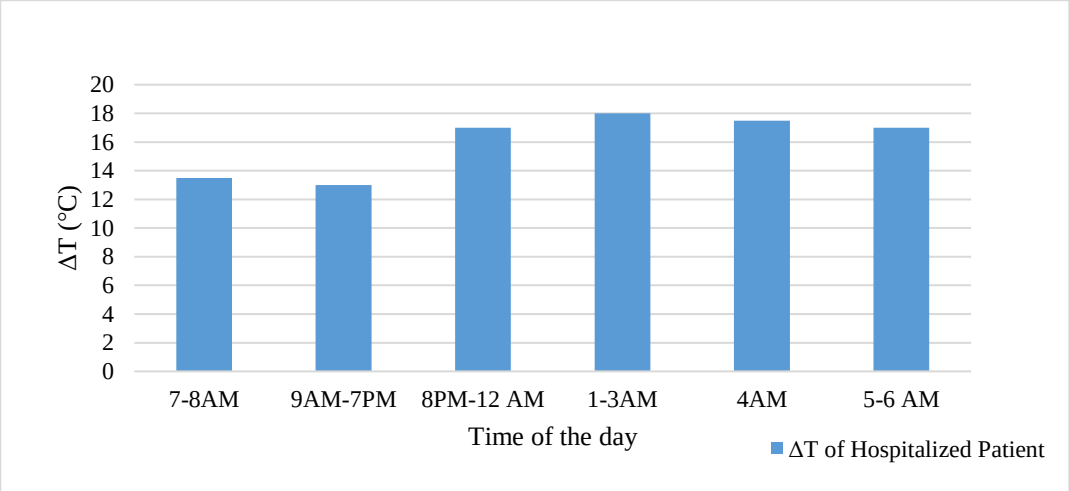

Figure 4.5. ΔT for hospitalized patient with no movement

From the table, the amount of power harvested from the piezoelectric source when there is no frequency up conversion is very low and does not give the system much incentive in terms of power produced. Therefore, the case of the hospitalized patient with no movement and when the system has no FUC have increased levels of gradient temperature adjustments to allow the system to harvest enough power for system to support the loads autonomously.

The hospitalized patient case demonstrates that it is possible to power the system using only the thermoelectric harvester. However, in the other cases when the system

relied on the hybrid harvester, it was observed that the adjustments in the ambient temperature were lower. This justifies the inclusion of the piezoelectric source in movement-available scenarios to save on electricity cost that arises with specific air conditioning for ambient temperature adjustments.

Table 4.5. HeMeS 24-hour activity profile and environmental constraints of a hospitalized patient

Time (24hours)	**Activity**	**Tbody**	**Tair**	**Frequency of motion**
7:00:00 AM	Medium	37.5	24	0
8:00:00 AM	Medium	37.5	24	0
9:00:00 AM	Medium	37	24	0
10:00:00 AM	Medium	37	24	0
11:00:00 AM	Medium	37	24	0
12:00:00 PM	Min	37	24	0
1:00:00 PM	Min	37	24	0
2:00:00 PM	Min	37	24	0
3:00:00 PM	Min	37	24	0
4:00:00 PM	Min	37	24	0
5:00:00 PM	min	37	24	0
6:00:00 PM	min	37	24	0
7:00:00 PM	Min	37	24	0
8:00:00 PM	No	37	20	0
9:00:00 PM	No	37	20	0
10:00:00 PM	No	37	20	0
11:00:00 PM	No	37	20	0
12:00:00 AM	No	37	20	0
1:00:00 AM	No	37	19	0
2:00:00 AM	No	37	19	0
3:00:00 AM	No	37	19	0
4:00:00 AM	No	37	19.5	0
5:00:00 AM	No	37	20	0
6:00:00 AM	No	37	20	0
Total (whole day)	Average	**37.04**	**22.02**	0

Table 4.6. Output power for the harvesters for different patient types

Patient type	**Condition**	**Piezo source**	**Freq. of motion**	**ΔT ºC**	**TEG power**
Non-critical patient	FUC enabled	425.2 µW	1.27 Hz	14.21	1.43 mW
	FUC disabled	3.285 µW	2.04 Hz	14.87	1.43 mW
Nursing home Patient	FUC enabled	47.11 µW	1 Hz	14.52	1.44 mW
	FUC disabled	1.090 µW	1.54 Hz	15	1.384 mW
Hospitalized patient	No movement	-	-	15.02	1.47 mW

4.2 User activity constrained analysis to determine maximum load activity

4.2.1 Patient with monitored biosignals and FUC is enabled

Different activity levels are simulated for a non-critical patient with frequency up conversion. The maximum activity levels for the loads for autonomous operation is as tabulated in Table 4.8. for a non-critical patient when frequency up conversion is enabled.

4.2.2 Patient with monitored biosignals and FUC disabled

In this case no frequency up conversion was implemented in the piezoelectric harvester. Without frequency up conversion, the piezo harvester produces very low

outputs. The hybrid harvester is now majorly dominated by the thermoelectric harvester. HeMeS applied for a patient with monitored biosignals and without FUC is tested for maximum activity level for autonomous operation. Table 4.9 shows the activity levels of the loads for this case.

When the two cases are compared, the case that has FUC enabled allows higher levels of activity in the system compared to when FUC is disabled. The reason for this is due to the lower generated power from the hybrid harvester when there is no FUC in the piezo source.

4.2.3 Nursing home patient with FUC enabled

Nursing home patients are mostly the elderly, and their level of motion is quite low therefore lower activity levels are achieved in the loads unlike in cases when the patient have higher levels of movement. The maximum activity levels for the loads for autonomous operation for a nursing home patient using HeMeS are summarized in Table 4.10.

4.2.4 Nursing home patient with FUC disabled

When there is no frequency up conversion, the overall amount power harvested by the tool is low and therefore the activity levels are even more reduced than in the case with FUC reduced. Table 4.11 shows the maximum achievable activity level in this case.

4.2.5 Hospitalized patient

In the case of a hospitalized patient, a no movement case is assumed and therefore the piezoelectric source does not contribute to the total power harvested. In this case the TEG is the main source consequently. The maximum activity level for autonomous operation for a hospitalized patient is summarized in Table 4.12.

Table 4.7. HeMeS maximum load activity level for 24 hr. autonomous operation: Monitored patient with FUC

Module	**Origin**	**State**	**%Time**	**Supply current**
Ultra-low-power 32-bit MCU Arm®-based Cortex®-M3	Infineon	Active	15%	60 µA
		Idle	85%	2 µA
BLE	On Semiconductor	Rx	3%	3.3 mA
		Tx	3%	3.2 mA
		Idle	94%	10 µA
Temperature sensor	Bosch Sensortec	Active	100%	3 µA
ADXL 345	Analog Devices	Active	100%	30 µA
Pulse rate sensor	Bosch Sensortec	Active	11%	100 µA
		Idle	89%	1 µA
EPIC Ultra High Impedance ECG Sensor	Plessey Semi-conductors	Active	4%	2.5 mA
		Idle	96%	10 nA

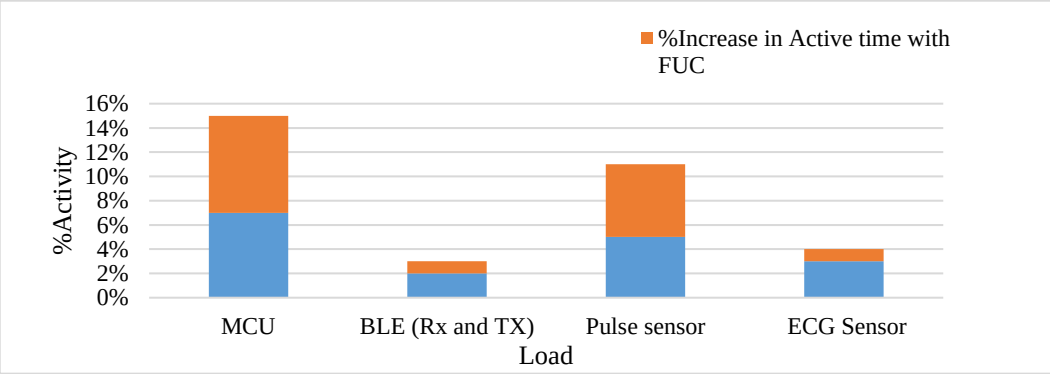

Figure 4.6. % Load activity of non-critical patient with monitored biosignals for case with FUC enabled and FUC disabled case.

Table 4.8. HeMeS maximum load activity level for 24 hr. autonomous operation: Monitored patient without FUC

Module	Origin	State	%Time	Supply current
Ultra-low-power 32-bit MCU Arm®-based Cortex®-M3	Infineon	Active	7%	60 µA
		Idle	93%	2 µA
BLE	On Semiconductor	Rx	2%	3.3 mA
		Tx	2%	3.2 mA
		Idle	96%	10 µA
Temperature sensor	Bosch Sensortec	Active	100%	3 µA
ADXL 345	Analog Devices	Active	100%	30 µA
Pulse rate sensor	Bosch Sensortec	Active	5%	100 µA
		Idle	95%	1 µA
EPIC Ultra High Impedance ECG Sensor	Plessey Semi-conductors	Active	3%	2.5 mA
		Idle	96%	10 nA

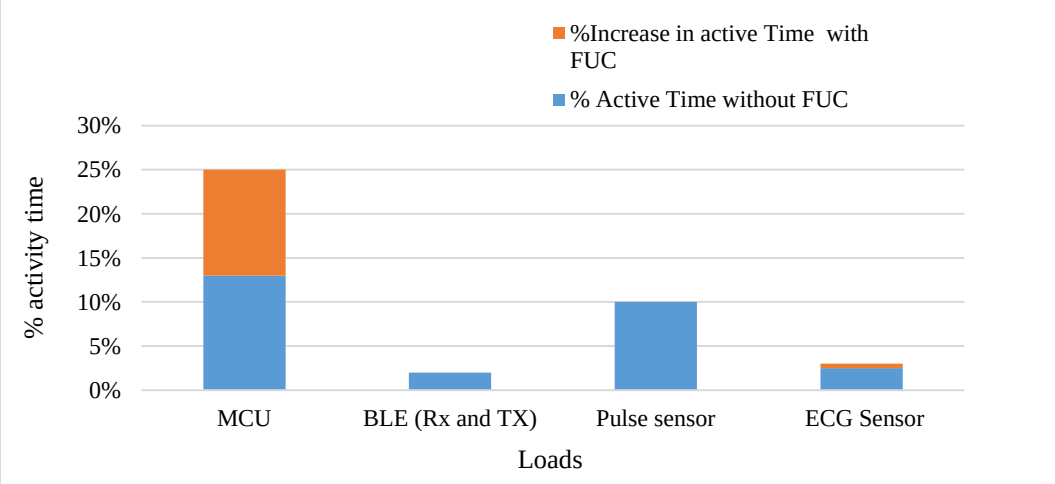

Figure 4.7. % Load activity of nursing home patient with monitored biosignals for case with FUC enabled and FUC disabled case

Table 4.9. HeMeS maximum load activity level for autonomous operation: Nursing home patient with FUC

Module	**Origin**	**State**	**%Time**	**Supply current**
Ultra-low-power 32-bit MCU Arm®-based Cortex®-M3	Infineon	Active	25%	60 µA
		Idle	75%	2 µA
BLE	On Semi-conductor	Rx	2%	3.3 mA
		Tx	2%	3.2 mA
		Idle	96%	10 µA
Temperature sensor	Bosch Sensortec	Active	100%	3 µA
ADXL 345	Analog Devices	Active	100%	30 µA
Pulse rate sensor	Bosch Sensortec	Active	10%	100 µA
		Idle	90%	1 µA
EPIC Ultra High Impedance ECG Sensor	Plessey Semi-conductors	Active	3%	2.5 mA
		Idle	97%	10 nA

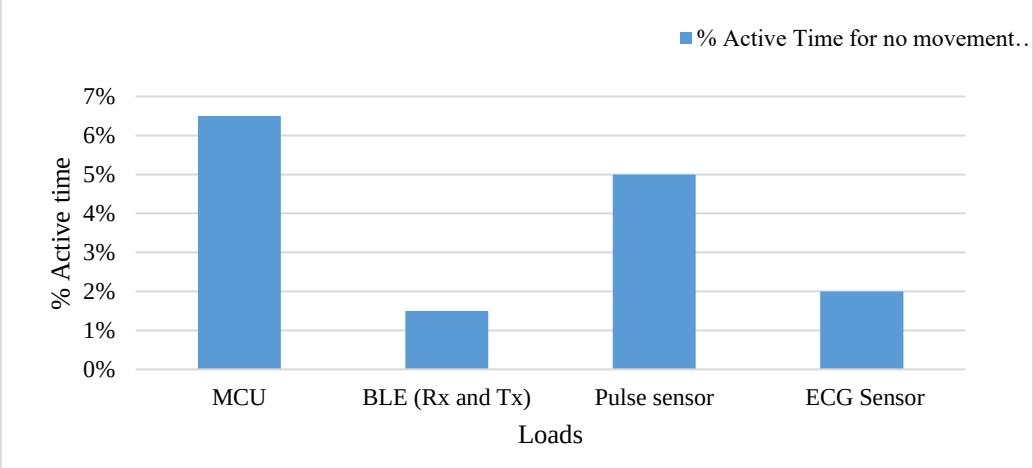

Figure 4.8. % Load active time for a hospitalized patient

Table 4.10. HeMeS activity level of loads for autonomous operation: Nursing home patient without FUC

Module	Origin	State	%Time	Supply current
Ultra-low-power 32-bit MCU Arm®-based Cortex®-M3	Infineon	Active	13%	60 µA
		Idle	87%	2 µA
BLE	On Semiconductor	Rx	2%	3.3 mA
		Tx	2%	3.2 mA
		Idle	96%	10 µA
Temperature sensor	Bosch Sensortec	Active	100%	3 µA
ADXL 345	Analog Devices	Active	100%	30 µA
Pulse rate sensor	Bosch Sensortec	Active	10%	100 µA
		Idle	90%	1 µA
EPIC Ultra High Impedance ECG Sensor	Plessey Semi-conductors	Active	2.5%	2.5 mA
		Idle	97.5%	10 nA

4.3 User and load activity constrained analysis to determine size

When movement, temperature, and WBAN node loads are fixed, a minimum system size for autonomous operation can be determined by doing a system sweep for various patient types. The size of the system includes the volume of constituent components but is mostly defined by the energy harvesters because the other components are a few millimeters in size. Additionally, the power generators i.e., the TEG and piezo components are the main determinants of whether the system operates autonomously since they provide system energy

Table 4.11. HeMeS activity level of loads for autonomous operation: Hospitalized patient

Module	**Origin**	**State**	**%Time**	**Supply current**
Ultra-low-power 32-bit MCU Arm®-based Cortex®-M3	Infineon	Active	6%	60 µA
		Idle	94%	2 µA
BLE	On Semiconductor	Rx	1.5%	3.3 mA
		Tx	1.5%	3.2 mA
		Idle	97%	10 µA
Temperature sensor	Bosch Sensortec	Active	100%	3 µA
ADXL 345	Analog Devices	Active	100%	30 µA
Pulse rate sensor	Bosch Sensortec	Active	5%	100 µA
		Idle	95%	1 µA
EPIC Ultra High Impedance ECG Sensor	Plessey Semi-conductors	Active	2%	2.5 mA
		Idle	98%	10 nA

Their sizes are a great determinant of how much energy is harvested from the system. Because the thermoelectric generator produces a considerable amount of power, its initially selected size was assumed optimal to keep the system within the required range for wearable application. The piezoelectric source on the hand can be adjusted to harvest more power in the system. Table 4.13 presents the power harvester sizes in volume.

Table 4.12. TEG and Piezo source sizes.

Description	Component	Volume
TEG source	TEG-126 LDT	8.16 cm^3
Piezo source	T220-H4BR-1305XB	0.2053 cm^3
Overall system size	HeMeS	10 cm^3

The piezoelectric sub-system is iterated to determine be the minimum system size (for sufficient piezoelectric power generation) for the system to operate autonomously. The system is optimized only for monitored patient and nursing home patient. The hospitalized patient is assumed to be in a no movement condition; therefore, the system size optimization applied to the piezoelectric source does not affect it. Table 4.14 and 4.15 show the optimum system sizes of the harvesters for cases when there is FUC and no FUC respectively for various patient types.

Table 4.13. Optimum size when there is frequency up conversion.

Application type	**Optimum piezo size**	**Overall system size**
Monitored patient	0.2053 cm^3	10 cm^3
Nursing home patient	0.468 cm^3	10.4 cm^3

Table 4.14. Optimum size without frequency up conversion

Application type	**Optimum Piezo size**	**Overall system size**
Monitored patient	1.367 cm^3	12 cm^3
Nursing home patient	1.583 cm^3	12 cm^3

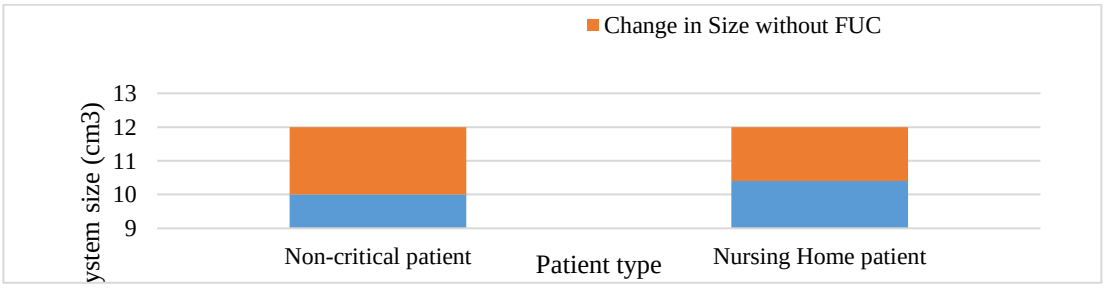

Figure 4.9. Optimum system size for autonomous operation with FUC enabled and EUC disabled

Table 4.16 summarizes the results of the design space exploration done with HeMeS. From this table the behavior of the system under different constraints is observed. It was observed that lower levels of activity are acceptable for all patient types when there is FUC in the system. In addition, the system allows higher levels of load activity when there is FUC. The downside of including FUC was the increase in system size due to including an additional piezoelectric harvester.

Table 4.15. Summary of design space exploration using HeMeS

Constrained parameter	**Variable parameter**	**Non-critical**			**Nursing home**			**Hospitalized**
		FUC enabled	FUC disabled	% Change in variable constraint	FUC enabled	FUC disabled	% Change in variable constraint	No movement
Load activity, System size	Frequency of movement	1.27 Hz	2.04Hz	↑ 60%	1 Hz	1.54 Hz	↑ 54%	-
	Temperature gradient	14.21° C	14.87° C	↑ 4.64%	14.52° C	15°C	↑ 3.30%	15.02°C
Patient movement, System size	MCU active time	15%	7%	↓ 53%	25%	13%	↓ 48%	6%
	BLE active time	3%	2%	↓ 33.30%	2%	2%	0%	1.50%
	ECG sensor active time	4%	3%	↓ 25%	3%	2.50%	↓ 16.70%	2%
	Pulse rate sensor active time	11%	5%	↓ 54%	10%	10%	0%	5%
Load activity, Patient movement	System size	10cm^3	12cm^3	↑ 20%	10.4cm^3	12cm^3	↑ 15.40%	10cm^3

CONCLUSIONS AND FUTURE WORK

5.1 Conclusions

Achieving complete autonomy in health monitoring devices necesitates that the power source does not hold the system back, and affords the system a sustainable level of reliability. This thesis presented some energy issues in WBANs and offered hybrid energy harvesting as an alternative to traditional depletable size constrained batteries. The thesis presented bio signals commonly monitored by various health sensors in multiparameter monitoring systems. The communication standards used for transmitting the measured bio signal to health care stations were also explored with specific attention to low power modules. Literature on the existing self-powered health monitoring systems was discussed to identify existing gaps. Afterwards, a health monitoring energy system tool, HeMeS, was developed to study the power flow from generation to load consumption in an autonomous system. Various system design scenarios were studied to demonstrate the strenghts of HeMeS in fast convergence in system design under a variety of constraints on the user side or load side. Sample analysis presented in this thesis included:

- Determination of minimum user activity when load activity is constrained
- Determination of maximum load activity when user activity is constrained
- Determination of minimum system size when both user and load activity are constrained

Some scenarios include non-critical patient, nursing home patient and hospitalized patient assumptions. In all the studied cases, selected independent variables are sweeped until an autonomous operation point is achieved. HeMeS has demonstrated that a hybrid thermal vibrational harvester system can be used to power a WBAN node continously for 24 hrs given that the environmental (user) conditions are matched to load requirements. Additionally, low power components and optimization of data processing and transmission rates are also important when

powering a system with energy harvesting. This thesis has demonstrated the possibility of moving toward sustainable clean energy sources for wearable health monitoring systems through systematic tools that cover multifaceted aspects of such systems.

HeMeS can be used for other design trade-offs for self-powered autonomous health monitoring device to determine the feasibility of various hybrid generation modes, applications enabled by new MEMS transducers and more efficient circuits, and new power management schemes. This approach ensures cost and size optimized autonomous solutions customized for patient or user categories.

This tool can be used in multi-disciplinary studies to co-design health monitoring nodes and energy harvester modules for accurately predicting energy flows and, to inform design choices based on the collective behavior of the components that make up a self-powered wearable body area network.

The adressed problem in this thesis is very relevant to the current state of affairs involving the battle to combat climate change and develop intelligent systems which are also sustainable by nature. HeMeS tool portion of the thesis was presented in [103]. Other portions of the thesis will be proliferated through one more conference and one journal paper.

Future work

Some suggestions for future work include

i. Expanding the hybrid system to include other harvesting techniques such as photovoltaic solar harvesting which will enable the expansion of system monitoring to outdoor conditions. The system can also be expanded to include electromagnetic energy harvesting if the system size requirement is relaxed. Incorporating more harvesters can lead to many more user capabilities.

ii. The code compatible version of the system that is automated can be part of the future work to allow for a quicker analysis in the design space exploration.

iii. HeMeS can be modified in the future to provide more information on why the result is not autonomous. More guidance to autonomy can be provided by the tool.

iv. Physical component models within HeMeS can be ported to a multi-physics platform such as COMSOL for increased accuracy

v. Finally, although the scope of the thesis was a high level system model, few design solutions that are obtained through HeMeS runs can be built and tested to increase confidence on results, and incorporate simulation-to-measurement correlation factors for improved accuracy.

REFERENCES

[1] S. Ullah *et al.*, “A Comprehensive Survey of Wireless Body Area Networks On PHY, MAC, and Network Layers Solutions,” pp. 1065–1094, 2012, doi: 10.1007/s10916-010-9571-3.

[2] A. Roy and B. H. Calhoun, “A 71 % Efficient Energy Harvesting and Power Management Unit for sub- ȝ W Power Biomedical Applications,” pp. 1–4, 2017.

[3] F. Akhtar and M. H. Rehmani, “Energy Harvesting for Self-Sustainable Wireless Body Area Networks,” *IT Prof.*, vol. 19, no. 2, pp. 32–40, 2017, doi: 10.1109/MITP.2017.34.

[4] Aqeel-ur-Rehman, Irfan Abdullah and S. U. Rehman, “Wireless Body Area Networks for Child Healthcare Monitoring : A Review,” 2018.

[5] M. A. Wahba, A. S. Ashour, and R. Ghannam, “Prediction of harvestable energy for self-powered wearable healthcare devices: Filling a gap,” *IEEE Access*, vol. 8, pp. 170336–170354, 2020, doi: 10.1109/ACCESS.2020.3024167.

[6] A. Tobola *et al.*, “Self-Powered Multiparameter Health Sensor,” *IEEE J. Biomed. Heal. Informatics*, vol. 22, no. 1, pp. 15–22, 2018, doi: 10.1109/JBHI.2017.2708041.

[7] I. Mahbub, S. A. Pullano, S. Shamsir, S. I. Kamrul, and S. A. Pullano, “Low-Power Wearable and Wireless Sensors for Advanced Healthcare Monitoring,” *IoT Low-Power Wirel.*, no. July, pp. 13–32, 2019, doi: 10.1201/9781351251662-2.

[8] T. L. Hayes, M. Pavel, and J. A. Kaye, “An unobtrusive in-home monitoring system for detection of key motor changes preceding cognitive decline,” *Annu. Int. Conf. IEEE Eng. Med. Biol. - Proc.*, vol. 26 IV, pp. 2480–2483,

2004, doi: 10.1109/iembs.2004.1403715.

[9] T. Jabeen, H. Ashraf, and A. Ullah, “A survey on healthcare data security in wireless body area networks,” *J. Ambient Intell. Humaniz. Comput.*, no. 2017, 2021, doi: 10.1007/s12652-020-02728-y.

[10] K. N. Qureshi, M. Q. Tayyab, S. U. Rehman, and G. Jeon, “An interference aware energy efficient data transmission approach for smart cities healthcare systems,” *Sustain. Cities Soc.*, vol. 62, no. April, p. 102392, 2020, doi: 10.1016/j.scs.2020.102392.

[11] H. Yu, N. Li, and N. Zhao, “How Far Are We from Achieving Self-Powered Flexible Health Monitoring Systems : An Energy Perspective,” vol. 2002646, pp. 1–11, 2021, doi: 10.1002/aenm.202002646.

[12] M. Kim, M. Kim, S. Lee, and C. Kim, “Wearable thermoelectric generator for harvesting human body heat energy,” no. 111, 2014, doi: 10.1088/0964-1726/23/10/105002.

[13] A. Pantelopoulos and N. G. Bourbakis, “A survey on wearable sensor-based systems for health monitoring and prognosis,” *IEEE Trans. Syst. Man Cybern. Part C Appl. Rev.*, vol. 40, no. 1, pp. 1–12, 2010, doi: 10.1109/TSMCC.2009.2032660.

[14] N. Gupta, *Inside Bluetooth Low Energy, Second Edition*. 2016.

[15] S. C. Ergen, “ZigBee/IEEE 802.15. 4 Summary,” *UC Berkeley, Sept.*, vol. 10, p. 17, 2004.

[16] I. Millar, M. Beale, B. J. Donoghue, K. W. Lindstrom, and S. Williams, “IrDA standards for high-speed infrared communications,” *Hewlett-Packard J.*, vol. 49, no. 1, pp. 10–26, 1998.

[17] M. N. Islam and M. R. Yuce, “Review of Medical Implant Communication System (MICS) band and network,” *ICT Express*, vol. 2, no. 4, pp. 188–194, 2016, doi: 10.1016/j.icte.2016.08.010.

[18] S. Pithadia, “Improving battery life in wearable patient monitors and medical patches,” pp. 1–6, 2019.

[19] S. M. Demir, F. Al-Turjman, and A. Muhtaroglu, “Energy Scavenging Methods for WBAN Applications: A Review,” *IEEE Sens. J.*, vol. 18, no. 16, pp. 6477–6488, 2018, doi: 10.1109/JSEN.2018.2851187.

[20] Y. W. Chong, W. Ismail, K. Ko, and C. Y. Lee, “Energy Harvesting for Wearable Devices: A Review,” *IEEE Sens. J.*, vol. 19, no. 20, pp. 9047–9062, 2019, doi: 10.1109/JSEN.2019.2925638.

[21] B. Ciftci, S. Chamanian, A. Koyuncuoglu, A. Muhtaroglu, and H. Kulah, “A Low-Profile Autonomous Interface Circuit for Piezoelectric Micro-Power Generators,” *IEEE Trans. Circuits Syst. I Regul. Pap.*, vol. 68, no. 4, pp. 1458–1471, 2021, doi: 10.1109/TCSI.2021.3053503.

[22] C. Yi, L. Wang, and Y. Li, “Energy Efficient Transmission Approach for WBAN Based on Threshold Distance,” vol. 15, no. 9, pp. 5133–5141, 2015, doi: 10.1109/JSEN.2015.2435814.

[23] J. Saraswat and P. P. Bhattacharya, “Effect of Duty Cycle on Energy Consumption in Wireless Sensor Networks,” *Int. J. Comput. Networks Commun.*, vol. 5, no. 1, pp. 125–140, 2013, doi: 10.5121/ijcnc.2013.5109.

[24] T. J. Voss, V. Subbian, and F. R. Beyette, “Feasibility of energy harvesting techniques for wearable medical devices,” *2014 36th Annu. Int. Conf. IEEE Eng. Med. Biol. Soc. EMBC 2014*, pp. 626–629, 2014, doi: 10.1109/EMBC.2014.6943669.

[25] J. Selvarathinam and A. S. Anpalagan, “Energy harvesting from the human body for biomedical applications,” no. December, pp. 6–12, 2016.

[26] C. Lu, V. Raghunathan, and K. Roy, “Efficient design of micro-scale energy harvesting systems,” *IEEE J. Emerg. Sel. Top. Circuits Syst.*, vol. 1, no. 3, pp. 254–266, 2011, doi: 10.1109/JETCAS.2011.2162161.

[27] S. A. Murawski, W. T. Hogarth, E. B. Peebles, and L. Barbeiri, “Prevalence of External Skin Lesions and Polycyclic Aromatic Hydrocarbon Concentrations in Gulf of Mexico Fishes, Post-Deepwater Horizon,” *Trans. Am. Fish. Soc.*, vol. 143, no. 4, pp. 1084–1097, 2014, doi: 10.1080/00028487.2014.911205.

[28] L. Mateu and F. Moll, “Review of energy harvesting techniques and applications for microelectronics,” no. June 2005, 2021, doi: 10.1117/12.613046.

[29] H. Uluşan, S. Chamanian, W. P. M. R. Pathirana, Zorlu, A. Muhtaroğlu, and H. Külah, “A triple hybrid micropower generator with simultaneous multi-mode energy harvesting,” *Smart Mater. Struct.*, vol. 27, no. 1, 2018, doi: 10.1088/1361-665X/aa8a09.

[30] U. Anliker *et al.*, “AMON: A wearable multiparameter medical monitoring and alert system,” *IEEE Trans. Inf. Technol. Biomed.*, vol. 8, no. 4, pp. 415–427, 2004, doi: 10.1109/TITB.2004.837888.

[31] A. Tobola *et al.*, “Battery Runtime Optimization Toolbox for Wearable Biomedical Sensors,” pp. 199–204, 2016.

[32] C. Lockwood *et al.*, “Vital signs,” pp. 207–230, 2004.

[33] J. Matos, R. Tung, and P. Zimetbaum, “Use of the electrocardiogram in acute myocardial infarction,” *Card. Intensive Care*, pp. 99-102.e1, 2018, doi: 10.1016/B978-0-323-52993-8.00010-2.

[34] E. Amidi *et al.*, “Role of blood oxygenation saturation in ovarian cancer diagnosis using multi-spectral photoacoustic tomography,” *J. Biophotonics*, vol. 14, no. 4, pp. 1–13, 2021, doi: 10.1002/jbio.202000368.

[35] G. Hefftner, W. Zucchini, and G. G. Jaros, “The Electromyogram (EMG) as a Control Signal for Functional Neuromuscular Stimulation—Part I: Autoregressive Modeling as a Means of EMG Signature Discrimination,”

IEEE Trans. Biomed. Eng., vol. 35, no. 4, pp. 230–237, 1988, doi: 10.1109/10.1370.

[36] C. E. M. van Beijsterveldt and G. C. M. van Bal, "Twin and family studies of the human electroencephalogram : a re v iew and a," *Biol. Psychol.*, vol. 61, no. 2002, pp. 111–138, 2002.

[37] P. Boissy, S. Choquette, M. Hamel, and N. Noury, "User-based motion sensing and fuzzy logic for automated fall detection in older adults," *Telemed. e-Health*, vol. 13, no. 6, pp. 683–693, 2007, doi: 10.1089/tmj.2007.0007.

[38] M. Sung, C. Marci, and A. Pentland, "Wearable feedback systems for rehabilitation," vol. 12, pp. 1–12, 2005, doi: 10.1186/1743-Received.

[39] B. Lin, B. Lin, N. Chou, F. Chong, and S. Chen, "RTWPMS : A Real-Time Wireless Physiological Monitoring System," vol. 10, no. 4, pp. 647–656, 2006.

[40] C. W. Mundt *et al.*, "A Multiparameter Wearable Physiologic Monitoring System for Space and Terrestrial Applications," vol. 9, no. 3, pp. 382–391, 2005.

[41] S. Saif, R. Saha, and S. Biswas, "On Development of MySignals based prototype for application in health vitals monitoring," *Wirel. Pers. Commun.*, no. 0123456789, 2021, doi: 10.1007/s11277-021-08963-6.

[42] M. S. Islam, M. T. Islam, A. F. Almutairi, G. K. Beng, N. Misran, and N. Amin, "Monitoring of the human body signal through the Internet of Things (IoT) based LoRa wireless network system," *Appl. Sci.*, vol. 9, no. 9, 2019, doi: 10.3390/app9091884.

[43] P. Rai *et al.*, "Smart healthcare textile sensor system for unhindered-pervasive health monitoring," no. March 2012, 2021, doi: 10.1117/12.921253.

[44] J. Habetha, "The MyHeart Project – Fighting Cardiovascular Diseases by Prevention and Early Diagnosis," pp. 6746–6749, 2006.

[45] R. Paradiso, G. Loriga, and N. Taccini, “A Wearable Health Care System Based on Knitted Integrated Sensors,” vol. 9, no. 3, pp. 337–344, 2005.

[46] R. Villar, T. Beltrame, and R. L. Hughson, “Validation of the Hexoskin wearable vest during lying, sitting, standing, and walking activities,” *Appl. Physiol. Nutr. Metab.*, vol. 40, no. 10, 2015, doi: 10.1139/apnm-2015-0140.

[47] C. Elliot, M. Hamlin, & C. L.-T. J. of S., and undefined 2019, “Validity and reliability of the hexoskin wearable biometric vest during maximal aerobic power testing in elite cyclists,” *journals.lww.com*, doi: 10.1519/JSC.0000000000002005.

[48] M. Di Rienzo *et al.*, “MagIC System : a New Textile-Based Wearable Device for Biological Signal Monitoring . Applicability in Daily Life and Clinical Setting,” pp. 7167–7169, 2005.

[49] Yang Hao and Robert Foster, “Wireless body sensor networks for health-monitoring applications,” 2008, doi: 10.1088/0967-3334/29/11/R01.

[50] C. Aleksandar Milenkovic´ , Otto and E. Jovanov, “Wireless sensor networks for personal health monitoring : Issues and an implementation,” *Elsevier*, vol. 29, pp. 2521–2533, 2006, doi: 10.1016/j.comcom.2006.02.011.

[51] and M. W. Shnayder, Victor, Bor-rong Chen, Konrad Lorincz, Thaddeus R. F. Fulford-Jones, “Sensor Networks for Medical Care,” 2005.

[52] M. R. Yuce, S. W. P. Ng, and N. L. Myo, “Wireless Body Sensor Network Using Medical Implant Band,” pp. 467–474, 2007, doi: 10.1007/s10916-007-9086-8.

[53] B. Gyselinckx, J. Penders, and R. Vullers, “Potential and challenges of body area networks for cardiac monitoring,” vol. 40, pp. 165–168, 2007, doi: 10.1016/j.jelectrocard.2007.06.016.

[54] W. Y. Chung, S. C. Lee, and S. H. Toh, “WSN based mobile u-healthcare system with ECG, blood pressure measurement function,” *Proc. 30th Annu.*

Int. Conf. IEEE Eng. Med. Biol. Soc. EMBS'08 - "Personalized Healthc. through Technol., pp. 1533–1536, 2008, doi: 10.1109/iembs.2008.4649461.

[55] S. Chamanian, B. Ciftci, H. Ulusan, A. Muhtaroglu, and H. Kulah, "Power-Efficient Hybrid Energy Harvesting System for Harnessing Ambient Vibrations," *IEEE Trans. Circuits Syst. I Regul. Pap.*, vol. 66, no. 7, pp. 2784–2793, 2019, doi: 10.1109/TCSI.2019.2900574.

[56] A. Muhtaroglu, A. Yokochi, and A. von Jouanne, "A sustainable power architecture for mobile computing systems," *J. Power Sources*, vol. 178, no. 1, pp. 467–475, 2008, doi: 10.1016/j.jpowsour.2007.11.007.

[57] M. F. Shaik, "Implementation of wearable glucose sensor node with energy harvesting for Wireless Body Area Network," pp. 2019–2022, 2019.

[58] D. C. Hoang, Y. K. Tan, H. B. Chng, and S. K. Panda, "Thermal energy harvesting from human warmth for wireless body area network in medical healthcare system," *Proc. Int. Conf. Power Electron. Drive Syst.*, pp. 1277–1282, 2009, doi: 10.1109/PEDS.2009.5385814.

[59] C. Covaci and A. Gontean, "Piezoelectric energy harvesting solutions: A review," *Sensors (Switzerland)*, vol. 20, no. 12, pp. 1–37, 2020, doi: 10.3390/s20123512.

[60] A. Vyas *et al.*, "Towards Integrated Flexible Energy Harvester and Supercapacitor for Self-powered Wearable Sensors," pp. 1–6, 2020, doi: 10.1109/powermems49317.2019.008.

[61] J. Zhao and Z. You, "Models for 31-mode PVDF energy harvester for wearable applications," *Sci. World J.*, vol. 2014, 2014, doi: 10.1155/2014/893496.

[62] H. Liu, J. Zhong, C. Lee, S. W. Lee, and L. Lin, "A comprehensive review on piezoelectric energy harvesting technology: Materials, mechanisms, and applications," *Appl. Phys. Rev.*, vol. 5, no. 4, 2018, doi: 10.1063/1.5074184.

[63] J. M. Muganda, B. Jansen, E. Homburg, Y. Van De Burgt, and J. Den Toonder, “the Direct and Indirect Piezoelectric Effect for Surface Shape Control in Adaptive Systems,” pp. 1–9, doi: 10.1109/TASE.2021.3053431.

[64] M. J. Ramsay and W. W. Clark, “<title>Piezoelectric energy harvesting for bio-MEMS applications</title>,” *Smart Struct. Mater. 2001 Ind. Commer. Appl. Smart Struct. Technol.*, vol. 4332, no. June 2001, pp. 429–438, 2001, doi: 10.1117/12.429684.

[65] E. B. Tadmor, G. Kósa, and A. Member, “Electromechanical Coupling Correction for Piezoelectric Layered Beams,” vol. 12, no. 6, pp. 899–906, 2003.

[66] P. Dziurdzia, “Modeling and Simulation of Thermoelectric Energy Harvesting Processes,” *Sustain. Energy Harvest. Technol. - Past, Present Futur.*, no. April, 2014, doi: 10.5772/28530.

[67] E. Kanimba and Z. Tian, “Modeling of a Thermoelectric Generator Device,” *Thermoelectr. Power Gener. - A Look Trends Technol.*, 2016, doi: 10.5772/65741.

[68] K. Pietrzyk, J. Soares, B. Ohara, and H. Lee, “Power generation modeling for a wearable thermoelectric energy harvester with practical limitations,” *Appl. Energy*, vol. 183, pp. 218–228, 2016, doi: 10.1016/j.apenergy.2016.08.186.

[69] W. Jin *et al.*, “Exploring Peltier effect in organic thermoelectric fi lms,” *Nat. Commun.*, pp. 1–6, 2018, doi: 10.1038/s41467-018-05999-4.

[70] M. Huang, R. Yen, and A. Wang, “The influence of the Thomson effect on the performance of a thermoelectric cooler,” vol. 48, pp. 413–418, 2005, doi: 10.1016/j.ijheatmasstransfer.2004.05.040.

[71] C. C. Maduabuchi, C. A. Mgbemene, and O. I. Ibeagwu, “Thermally Induced Delamination of PV-TEG : Implication of Leg ’ s Joule and Thomson Heating,” *J. Electron. Mater.*, vol. 49, no. 11, pp. 6417–6427, 2020, doi:

10.1007/s11664-020-08390-6.

[72] R. Zevenhoven and A. Beyene, “The relative contribution of waste heat from power plants to global warming,” *Energy*, vol. 36, no. 6, pp. 3754–3762, 2011, doi: 10.1016/j.energy.2010.10.010.

[73] T. S. state power Generators, “TEG2-126LDT for Body & Sensor Power Thermoelectric Harvesting Applications ! Specially designed TEG2-126LDT .,” pp. 4–5.

[74] Eurydice Kanimba and Zhiting Tian, “Modeling of a Thermoelectric Generator Device,” *IntechOpen*, 2016.

[75] A. Nozariasbmarz *et al.*, “High Power Density Body Heat Energy Harvesting,” *ACS Appl. Mater. Interfaces*, 2019, doi: 10.1021/acsami.9b14823.

[76] M. Ben Ammar, “Design of a DC-DC Boost Converter of Hybrid Energy Harvester for Low-Power Biomedical Applications,” pp. 955–959, 2020.

[77] Sayed Mohammad Noghabaei and Mohama Sawan, “A fully integrated High-Efficiency Step-up DC-DC converter fro energy Harvesting applications,” pp. 121–122, 2016.

[78] N. Badri, L. Nasraoui, L. A. Saidane, and S. Ikki, “Maximizing Lifetime in Energy-Harvesting WBSN for Health Monitoring Systems Through Dynamic Slots Allocation,” pp. 325–329, 2019.

[79] D. Fan, L. L. Ruiz, J. Gong, and J. Lach, “EHDC : An Energy Harvesting Modeling and Profiling Platform for Body Sensor Networks,” vol. 22, no. 1, pp. 33–39, 2018.

[80] L. Guo, S. Member, Z. Chen, and D. Zhang, “Sustainability in Body Sensor Networks With Transmission Scheduling and Energy Harvesting,” vol. 6, no. 6, pp. 9633–9644, 2019.

[81] T. Wu, F. Wu, J. M. Redoute, and M. R. Yuce, “An Autonomous Wireless Body Area Network Implementation Towards IoT Connected Healthcare Applications,” *IEEE Access*, vol. 5, no. July, pp. 11413–11422, 2017, doi: 10.1109/ACCESS.2017.2716344.

[82] A. Dionisi, D. Marioli, E. Sardini, and M. Serpelloni, “Autonomous Wearable System for Vital Signs Measurement With Energy-Harvesting Module,” *IEEE Trans. Instrum. Meas.*, vol. 65, no. 6, pp. 1423–1434, 2016, doi: 10.1109/TIM.2016.2519779.

[83] S. Chamanian, S. Baghaee, H. Ulusan, O. Zorlu, E. Uysal-Biyikoglu, and H. Kulah, “Implementation of Energy-Neutral Operation on Vibration Energy Harvesting WSN,” *IEEE Sens. J.*, vol. 19, no. 8, pp. 3092–3099, 2019, doi: 10.1109/JSEN.2019.2890902.

[84] H. Pl. and S. P. L. D. FLu, “Modeling and analysis of micro piezoelectric power generators for micro- electromechanical-systems applications,” no. June 2014, 2004, doi: 10.1088/0964-1726/13/1/007.

[85] A. S. Herbawi, O. Paul, and T. Galchev, “An Ultra-Low-Power Active AC-DC CMOS Converter For Sub-1V Integrated Energy Harvesting Applications,” pp. 1–4, 2013.

[86] H. Oon, C. Houng, S. Sarah, S. Parasuraman, and M. K. A. A. Khan, “Energy Harvesting From Human Locomotion : Gait Analysis , Design and state of art,” vol. 42, pp. 327–335, 2014, doi: 10.1016/j.procs.2014.11.070.

[87] A. Khan, “Modeling and Simulation of Solar Energy Harvesting Systems with Artificial Neural Networks,” 2013.

[88] MIDE, *PIEZO.COM Materials Technical Data*. 2020, p. 1.

[89] T. Eggborn, “Analytical Models to Predict Power Harvesting with Piezoelectric Materials,” *Masters Thesis, Virginia Polytech. Inst. State Univ. VA Frederick, A. A., Clark, W. W., Hu, H*, vol. 5, no. May, p. 11, 2003.

[90] M. Gomez, B. Ohara, R. Reid, and H. Lee, “Investigation of the Effect of Electrical Current Variance on Thermoelectric Energy Harvesting,” vol. 43, no. 6, pp. 1744–1751, 2014, doi: 10.1007/s11664-013-2854-y.

[91] Shashank Priya · Daniel J. Inman, *Energy Harvesting Technologies*. Springer US, 2009.

[92] Eaton, “Eato PowerStor Supercapacitors,” no. December 2011, pp. 2015–2017, 2016.

[93] Plessey Semiconductors, “EPIC Ultra High Impedance ECG Sensor Advance Information,” no. 2, pp. 1–6, [Online]. Available: www.plesseysemi.com.

[94] ST, “Ultra-low-power 32-bit MCU Arm®-based Cortex®-M3 with 512KB Flash, 80KB SRAM, 16KB EEPROM, LCD, USB, ADC, DAC,” no. April, 2021.

[95] World Famous Electronics Ilc, “Pulse Sensor Guide,” 2016.

[96] M. A. Halim, H. O. Cho, and J. Y. Park, “A handy motion driven, frequency up-converting piezoelectric energy harvester using flexible base for wearable sensors applications,” *2015 IEEE SENSORS - Proc.*, 2015, doi: 10.1109/ICSENS.2015.7370437.

[97] N. Georgi and R. Le Bouquin Jeannes, “Proposal of a remote monitoring system for elderly health prevention,” *2017 Int. Conf. Smart, Monit. Control. Cities, SM2C 2017*, pp. 69–74, 2017, doi: 10.1109/SM2C.2017.8071261.

[98] N. Stefanos, D. D. Vergados, and I. Anagnostopoulos, “Health care information systems and personalized services for assisting living of Elderly people at nursing home,” *Proc. - 3rd Int. Work. Semant. Media Adapt. Pers. SMAP 2008*, pp. 122–127, 2008, doi: 10.1109/SMAP.2008.36.

[99] F. M. Jansen, G. H. Van Kollenburg, C. B. M. Kamphuis, F. H. Pierik, and D. F. Ettema, “Hour-by-hour physical activity patterns of adults aged 45-65 years: A cross-sectional study,” *J. Public Heal. (United Kingdom)*, vol. 40,

no. 4, pp. 787–796, 2018, doi: 10.1093/pubmed/fdx146.

[100] A. F. B. F. P. Denilson de Castro TEIXEIRA, Nidia Aparecida HERNANDES, Vanessa Suziane PROBST, Ercy Maria Cipulo RAMOS, “Profi le of physical activity in daily life in physically independent elderly men and women,” pp. 645–655, 2012.

[101] B. Maamer, A. Boughamoura, A. M. R. Fath El-Bab, L. A. Francis, and F. Tounsi, “A review on design improvements and techniques for mechanical energy harvesting using piezoelectric and electromagnetic schemes,” *Energy Convers. Manag.*, vol. 199, no. February, p. 111973, 2019, doi: 10.1016/j.enconman.2019.111973.

[102] N. Tekbıyık Ersoy, “EFFICIENT RESOURCE ALLOCATION IN ENERGY HARVESTINGWIRELESS NETWORKS,” vol. 148, pp. 148–162.

[103] M. Sharone and A. Muhtaroglu, “HeMeS : Autonomous Health Monitoring Energy System Tool for Design of Self-Sustained WBANs,” Proceedings of 6th *International Conference on Intelligent Informatics and Biomedical Sciences (ICIIBMS)*, 2021 (Accepted**)**.

APPENDICES

A. Supercapacitor power when in autonomous operation

(Shown as a representation due to too many graphs from iterations)

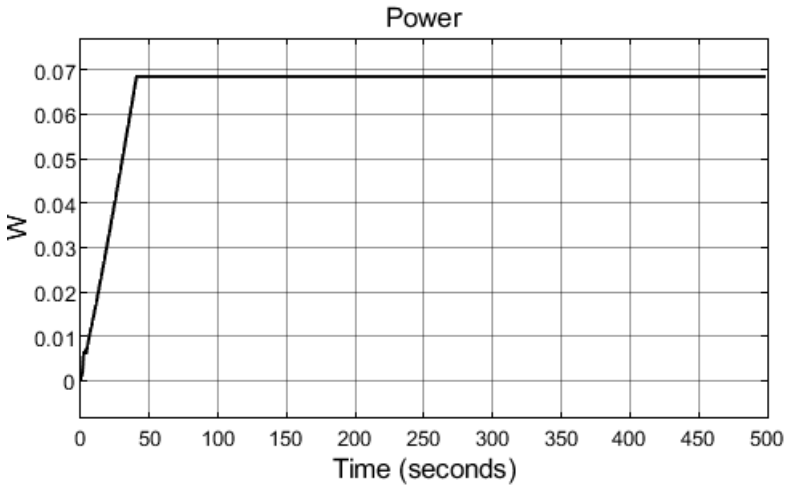

B. HeMeS code for obtaining ΔT of the TEG

```
%function
function F=myfun(T)

% Non-critical patient(24 hrs average)
Noncriticalpatient_ActivityData=xlsread('Normal.xlsx');
BodyTemperature=Noncriticalpatient_ActivityData(25,3);
AmbientTemperature=Noncriticalpatient_ActivityData(25,4
);

% Nursing home patient(24 hrs average)
Nursinghomepatient_ActivityData=xlsread('Elderly.xlsx')
;
BodyTemperature=Nursinghomepatient_ActivityData(25,3);
AmbientTemperature=Nursinghomepatient_ActivityData(25,4
);

%Hospitalized patient (24 hrs average)
```

```
Hospitalizedpatient_activityData=xlsread('Hospitalized.
xlsx');
BodyTemperature=Hospitalizedpatient_activityData(25,3);
AmbientTemperature=Hospitalizedpatient_activityData(25,
4);

As=16*(10^-4);%Module surface area
K=1.820;%Thermoelectric thermal conductivity
B=0.0336;%leg length dived by fill factor
alphaP=186*(10^-6);%Seebeck Coefficient of ptype
semicoductor leg
alphaN=-186*(10^-6);%Seebeck Coefficient of ntype
semicoductor leg
rho= 7.226*(10^-6);%is the electrical resistance of the
thermoelectric material
T_body=BodyTemperature;
T_ambient=AmbientTemperature;
Thermal_R_Body=3.218;
Thermal_R_Heatsink=21.74;
%F here represent the Qh and Qc which are the heat
absorbed at the hot side
%and heat absorbed at the cold side respectively,
%Using heat conservation, the quantity of heat
transfered by joule
%heating,the peltier effect and heat conduction is
equal to heat trasfered
%from the heat source to the heat sink
F=[((As*K)/B)*(T(1)-T(2))+((((alphaP-
alphaN)^2)*As*(T(1)-T(2)))/(4*B*rho*2))*T(1)-
((As/8*B*rho)*(((alphaP-alphaN)*(T(1)-T(2)))/2)^2)-
(T_body-T(1))/Thermal_R_Body;
((As*K)/B)*(T(1)-T(2))+((((alphaP-alphaN)^2)*As*(T(1)-
T(2)))/(4*B*rho*2))*T(2)+((As/8*B*rho)*(((alphaP-
alphaN)*(T(1)-T(2)))/2)^2)-(T(2)-
T_ambient)/Thermal_R_Heatsink];
end
```

TEZ İZİN FORMU / THESIS PERMISSION FORM

PROGRAM / PROGRAM

Sürdürülebilir Çevre ve Enerji Sistemleri / Sustainable Environment and Energy Systems	☑
Siyaset Bilimi ve Uluslararası İlişkiler / Political Science and International Relations	☐
İngilizce Öğretmenliği / English Language Teaching	☐
Elektrik Elektronik Mühendisliği / Electrical and Electronics Engineering	☐
Bilgisayar Mühendisliği / Computer Engineering	☐
Makina Mühendisliği / Mechanical Engineering	☐

YAZARIN / AUTHOR
Soyadı / Surname : SHARONE
Adı / Name : MOLLY
Programı / Program : SEES

TEZİN ADI / TITLE OF THE THESIS (**İngilizce** / English) : ENERGY MODELING OF WEARABLE INTELLIGENT BATTERYLESS HEALTH MONITORING SYSTEM WITH THERMAL-VIBRATIONAL HYBRID HARVESTER

TEZİN TÜRÜ / DEGREE: **Yüksek Lisans** / Master ☑ **Doktora** / PhD ☐

1. **Tezin tamamı dünya çapında erişime açılacaktır. /** Release the entire work immediately for access worldwide. ☐

2. **Tez <u>iki yıl</u> süreyle erişime kapalı olacaktır.** / Secure the entire work for patent and/or proprietary purposes for a period of **<u>two years</u>**. * ☐

3. **Tez <u>altı ay</u> süreyle erişime kapalı olacaktır.** / Secure the entire work for period of **<u>six months</u>**. * ☑

Yazarın imzası / Author Signature ..... **Tarih** / Date 18.09.2021

Tez Danışmanı / Thesis Advisor Full Name: PROF. DR. ALI MUHTARĞLU

Tez Danışmanı İmzası / Thesis Advisor Signature: .....

Eş Danışmanı / Co-Advisor Full Name: N/A

Eş Danışmanı İmzası / Co-Advisor Signature: N/A

Program Koordinatörü / Program Coordinator Full Name: ASST. PROF. DR. CEREN İNCE DEROGAR

Program Koordinatörü İmzası / Program Coordinator Signature: .....